STUDY OF PRESSURE LOSSES AT MAIN MINE FAN INSTALLATIONS USING COMPUTATIONAL FLUID DYNAMICS

by

Muhammad Mehdi

A thesis submitted to the faculty of
The University of Utah
in partial fulfillment of the requirements for the degree of

Master of Science

Department of Mining Engineering

The University of Utah

May 2016

Copyright © Muhammad Mehdi 2016

All Rights Reserved

STATEMENT OF THESIS APPROVAL

The thesis of **Muhammad Mehdi**

has been approved by the following supervisory committee members:

Felipe Calizaya	, Chair	**8-14-2015** Date Approved
Michael Nelson	, Member	**8-14-2015** Date Approved
James R. Stoll II	, Member	**8-14-2015** Date Approved

and by **Michael Nelson** ,Chair/Dean of

the Department/College/School of **Mining Engineering**

and by David B. Kieda, Dean of The Graduate School.

ABSTRACT

U.S. federal regulations pertinent to surface fan installation are concerned with mine safety and give little attention to the aerodynamic design of the installation. As a result, pressure drops has been reported at the installation. Ventilation surveys have shown that these pressure drops could be as high as 40% of fan pressure. The purpose of this study is to identify the sources for such a pressure drop and to reduce it.

In recent years, computational fluid dynamics (CFD) software has been successfully used in visualizing the fluid flow for different flow paths (geometries) subject to obstructions. CFD modeling is based on fluid flow principals. They are also applicable to mine ventilation. ANSYS FLUENT, a CFD software, was used as a research tool in this study.

A blower and an exhaust system were studied. For the former, using real mine data, the major sources of pressure loss were identified and parametric studies undertaken to minimize those losses. The losses are due to poor installation design with abrupt changes in air velocity and flow direction. Parametric analysis proved that the distance of the fan from any major obstruction is important. Installing the fan at a distance of at least twice the inlet duct diameter reduces the flow separation and formation of eddies.

For the exhaust system, it was found that the geometry of the evasée plays an important role in reducing the pressure losses; for instance, a conical evasée recovers the static pressure of the fan better than a rectangular evasée. This is due to the fact that a

rectangular evasée is subjected to shock losses. It is also found that the evasée must be of sufficient length so that the air is fully developed before it is discharged into the atmosphere. A proper transition piece between the fan outlet and the evasée is required.

This study has certain drawbacks and limitations. Due to limited computation-memory, no mesh-independent and y-plus tests were performed in the simulations. Mesh sizes were kept constant along with enhanced wall treatment which was used for all simulations.

Dedicated to Imam Raza (A.S.)

CONTENTS

LIST OF TABLES

LIST OF FIGURES

ACKNOWLEDGEMENTS

I would like to thank the Fulbright Program for their funding and support. This study would not have been possible without their funding. I would also like to thank Dr. Felipe Calizaya for his patience and devotion in supporting my research. Now that I am finished with my research, I realize that more than once, his “No” dragged me from my comfort zone into my learning zone. Also, thanks to Dr. Mike Nelson for providing all the resources required for this research. The findings of this research would not have been possible without his support, knowledge, and guidance. In addition, I would like to thank Dr. Rob Stroll for believing in me and serving on my thesis committee. His course on fluid dynamics made me more curious about the unpredictable and random nature of fluid behavior.

Furthermore, I would like to extend my thanks to all faculty members and students in the mining engineering department. Their moral support helped me to complete this research. Also, sincere thanks to Pam and Sam for their help. Also, many thanks to the Tiffany from the Graduate Writing Center for her support and humility.

Last but not least, I would like to thank my parents, my father- and mother- in law, and my siblings for their constant care, love, and prayers. Special thanks to love of my life, Rukhsana Mehdi, for being my heart, my conscious, and my confidante. I miss you all and hope to meet you all alive one day.

CHAPTER 1

INTRODUCTION

The ventilation requirements of a mine do not remain constant thoughout the mine's life. At the production stage of the mine, the mining activities intensify along with the increase in the mine development. Due to this reason, the ventilation requirements increase exponentially. There are several options to meet these requirements. One of these options is to increase the fan operating pressure. However, operating the main fans at higher pressure creates safety hazards and may damage bulkheads, stoppings, and air-lock doors. Hence other alternative options such as developing new mine openings, increasing the area of the airways, and modifying the ventilation system should be investigated. These alternative options require halting the production of the mine.

In this chapter, pressure losses associated with the fan house installation are discussed. The magnitude of these loses is significant. A proper fan installation design will minimize the shock losses. The pressure recovered by minimizing the shock losses will in turn increase the intake air quantity.

1.1 Problem Statement

Underground mines depend on surface and booster (fans that are installed inside a mine) fans for ventilation. Deep underground mines need mechanical devices such as

fans to move the air through the mine openings and remove the air contaminants. These devices generate pressure forces to overcome friction and shock losses.

Main fan installation follows the guidelines provided by the MSHA[1] (Mine Safety and Health Administration). Some of these are further discussed in Chapter 2. The main purpose of MSHA's guidelines is to enforce the mandatory safety standards. Following these guidelines does not necessarily ensure an aerodynamic fan installation design. Therefore, most of the fan installations in the United States are relatively safe but subjected to different shock losses. In some cases, these losses can be as high as 40 % of the static pressure developed by the fan. This problem is further discussed in the following section.

1.2 Problem Illustration

The air stream in a typical fan installation for an underground coal mine is subject to obstructions due to sudden change in air direction. For example, consider the exhaust system shown in Figure 1.1. Note that in the exhaust system, the air enters the mine through the mine portal and is exhausted into the atmosphere (refer to Chapter 3 for more detail).

This fan installation consists of the surface exhaust fan and fan installation components, including the fan ducts, evasée, and fan house. This design complies with the code of federal regulations, but it is not an appropriate installation and is subject to shock losses due to changes in cross-section area and changes in air flow direction.

---

[1]MSHA is administered by the Department of Labor. It deals with the regulations based on the Federal Mine Safety and Health Act of 1977 and subsequent legislation.

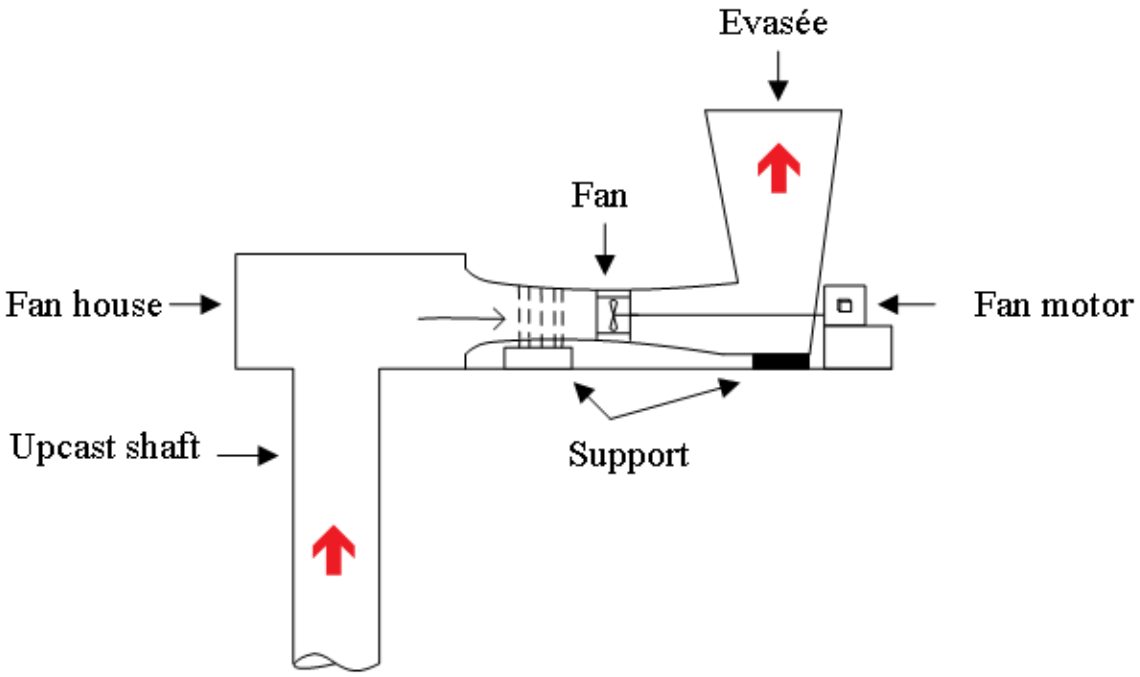

Figure 1.1 Typical surface fan installation

A fan survey was conducted by a ventilation team of the University of Utah for the installation shown in Figure 1.1. The main purpose of the survey was to calculate the amount of shock losses for this fan installation.

Survey data shown in Table 1.1 were obtained by measuring static and total pressure using pitot-static tube and manometer. Total and static pressure tests were performed at the fan installation and at the bottom of the shaft (Figure 1.2). This technique is further explained in Chapter 4.

The air quantity was calculated by determining the velocity pressure and inlet duct diameter. This velocity pressure is determined by subtracting total pressure from the static pressure.

The diameter of the upcast shaft is 4.5 m and it is 154 m in length. The resistance of the shaft was estimated to be equal to 0.00249 Ns^2/m^8.

Table 1.1 Summary of ventilation survey

Descriptions	Dimensions/ Measurements
Fan diameter	3.35 m
Fan pressure	3400 Pa
Fan quantity	415 m^3/s
Fan power	1410 kW
Shaft diameter	4.5 m
Shaft length	154 m
Bottom of the shaft across the stopping	1,300 Pa

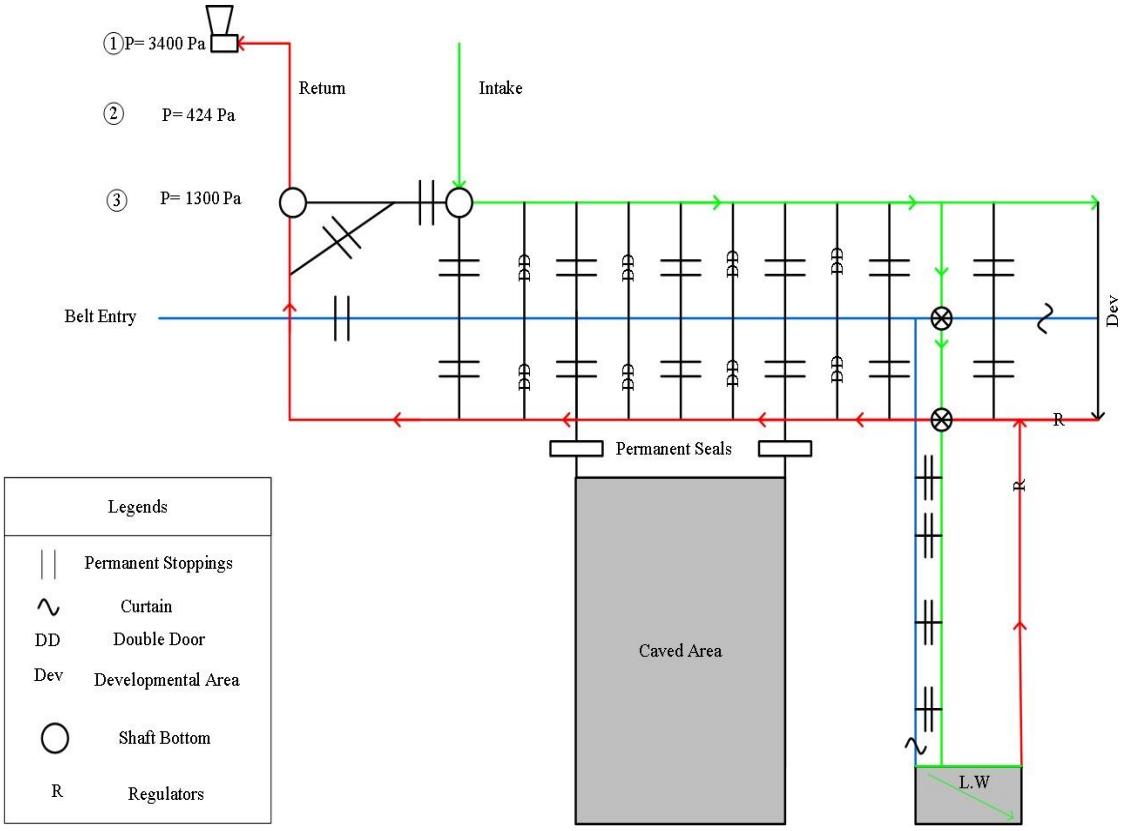

Figure 1.2 Schematic mine ventilation map with surveyed area

A total quantity of 415 m^3/s of air is exhausted through the shaft and the frictional pressure drop was calculated as:

$$P = 415^2 \times 0.00246 = 424 \text{ Pa}$$

During the survey, the differential pressure across a stopping separating the intake and return airways at the bottom of the shaft was measured at 1,300 Pa (see Figure 1.2). Based on the above data, the pressure loss due to the shock losses at the fan installation is estimated at:

$$P_{shock} = 3400 - 1300 - 424 = 1{,}676 \text{ Pa}$$

As mentioned earlier, these fan survey data came from the University of Utah ventilation research group in 2012. Part of this pressure loss can be recovered by

improving the fan house design and reducing the shock losses. Research is needed to identify the critical energy losses and produce alternate fan installation designs to minimize the shock losses.

1.3 Thesis Objectives

The main objective of the thesis is to quantify the pressure losses at or near the main surface fan installation. These losses are mainly the result of poor design of the fan house and main components. Different fan installation designs are developed to study the airflow behavior and minimize the pressure losses associated with this installation. Computational fluid dynamics (CFD) is used for this purpose. Three-dimensional (3-D) models, representing the various obstructions at the fan house, were simulated using ANSYS FLUENT software. The data obtained from these simulation studies were then put to the test to determine the effect of various fan installation components on the fan pressure. The governing principles of CFD, such as conservation of mass, momentum, and energy, are also discussed.

CHAPTER 2

LITERATURE REVIEW

Surface fans in U.S. coal mines are installed to comply with the federal regulations mostly concerned with safety issues and pay little attention to the aerodynamic design of the fan installation. It has been found that the exhaust fans are installed at a 90° angle with the main return shaft and short fan inlet ducts. Sometimes, due to space limitations, these are equipped with inadequate contraction and expansion cones. A significant percentage of fan energy is lost due to these obstructions. In this chapter, applicable federal regulations, fan system components, common types of fan installation, and common problems observed in fan installation are discussed.

2.1 Code of Federal Regulation for Fan Installations

The Code of Federal Regulations 30, part 75.310, pertaining to fan installations, mandates:

1. The mine fan needs to be installed on the surface in an incombustible housing.
2. Incombustible fan duct work should be used for the fan installation.
3. The fan operator shall always be at the surfaces location where the fan is installed.
4. The fan shall be offset by at least 4.57 m from the nearest side of the mine or shaft opening.

5. The fan shall be protected by one or more weak walls or explosion doors.

6. The area of the weak wall or explosion doors shall have a cross-sectional area equal to that of the mine opening.

7. Automatic monitoring devices shall be provided to report any abnormality.

8. Coal or other solid material between the pressure relief entry and the fan shall be at least 232 m^2.

9. In mines ventilated by multiple fans, an incombustible door shall be provided to prevent possible air-reversals.

10. The fan entry shall not be in direct line with a possible explosion.

2.2 Main Fan System Components

A main fan system consists of many components, including fan house, weak walls, fan parts, self-closing doors, and shaft collar design. The aerodynamic design of each one of these components is imperative for eliminating any unfavorable flow conditions. Each of the components is briefly discussed below.

2.2.1 Weak Wall

The Code of Federal Regulations, Title 30, Part 75.310 specifies that each fan shall be protected by at least one weak wall, also known as the explosion door. These weak walls provides a comparable degree of safety to the fan and housing from explosion waves.

In Figure 2.1, the projected area shows a typical weak wall installation. The sharp 90 ° offset is common in most of the main fan installations. The 90° configuration causes

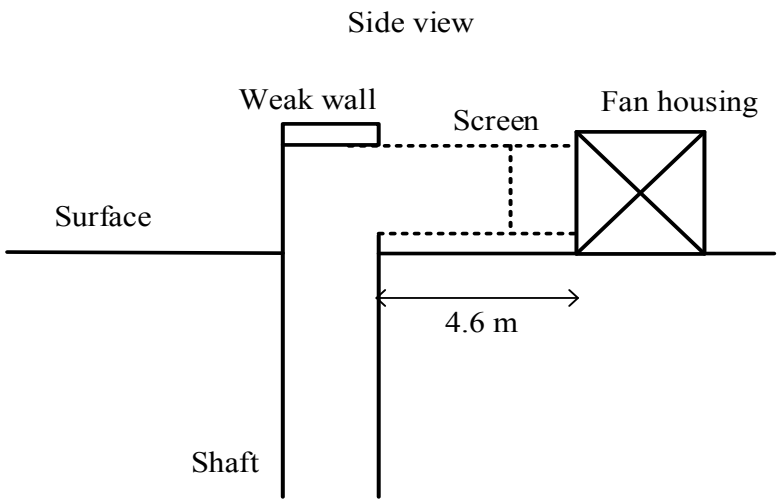

Figure 2.1 Standard weak wall fan installation

major shock losses. In practice, where terrain would not obstruct, a 90° configuration should be avoided in order to minimize shock losses. However, a distance greater than or equal to the 4.6 m is the legal requirement for offsetting the fan from the nearest side of the mine opening. It is also recommended to use added weak walls and a double fan screen (Figure 2.2). The purpose of the extended wall and screen is to provide debris with an exit before it reaches the surface fan (John 1993).

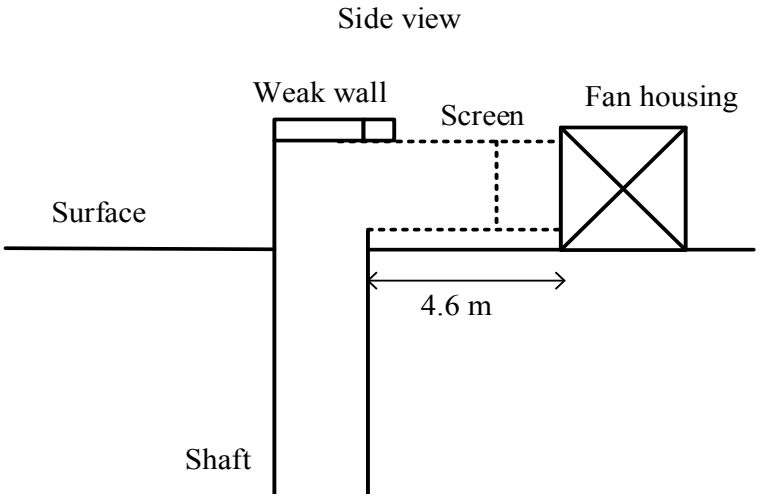

Figure 2.2 Recommended weak wall fan installation

2.2.2 Shaft Collar

The main function of the shaft collar is to provide the foundation to support the head frame of a shaft. Studies have shown that the shaft collar provides a smooth airflow transition for the change in direction of airflow at the top of the shaft (Ray 1997). It does not, however, completely negate the shock losses generated due to the sharp 90° turn between the shaft and the fan duct.

Field measurements by Ray (1997) showed that rounded roll-out incorporated onto the top of the shaft has low pressure loss coefficient on the order of –0.43 to +0.43 for a 1.83 m shaft, compared to 0.95 to 1.0 for sharp-edged collars. In mines where it is impossible to install a collar roll out at the top of the shaft, turning vanes (refer to Figure 2.3) can be retrofitted with the shaft. In fan installations, turning vanes are metal sheets that split the flow of air and are helpful in stabilizing the flow of air as it exits the mine shaft and enters the fan house.

Figure 2.3 shows turning vanes incorporated for parallel fan installations. The splitter plate isolates the two fans. The turning vanes are hinged to enable the section of vanes to extend over the shaft (Ray 1997). This will ensure that the turning vanes are lifted up in case of explosion.

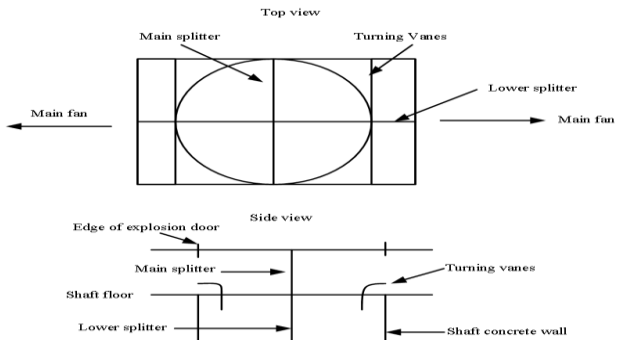

Figure 2.3 Top and side view of turning vanes for parallel fan installation

2.2.3 Ductwork Arrangement for Parallel Fan Installation

When a fan cannot deliver the required air quantity, the concept of using fans in parallel or parallel installation configuration is considered. Using fans in series or parallel preludes the use of a large main fan. In parallel installation, the fans are installed side by side. This results an increase in air quantity. In series, the fans are installed one after another. This type of installation results in an increase in fan power.

When fans are in parallel, each fan needs its separate duct. It has been found that fans at opposite sides of the mine opening are the least efficient. Since the fans are working in parallel and are installed at opposite sides, it may cause excessive turbulence when both fans are operating at the same time (Ray 1997).

In 1990, studies performed by the DMT[1] company for mine ventilation and climatology in Germany recommended an alternative ductwork and fan arrangement for parallel fans. The recommended arrangement is shown in Figure 2.4. This arrangement has a stable monometer column as it eliminates the "pumping" action produced by parallel fans.

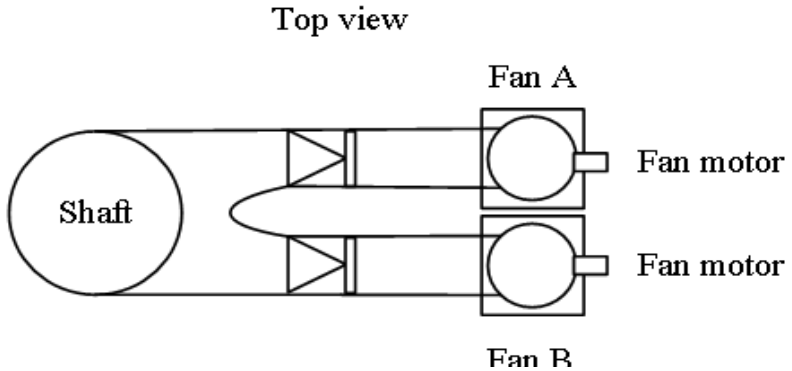

Figure 2.4 Ductwork arrangement for parallel fan installation

[1] DMT is an engineering and consulting company located in Germany.

2.3 Types of Fan

Two types of fans are commonly used in the mining industry: axial fans and centrifugal fans. In axial fans, the air moves in an axial direction by the tangential motion created by the rotating impeller of the fan. The main advantage of the axial fans is that they are portable and can easily be combined into series configurations. In centrifugal fans, the air enters the impeller axially and is accelerated by the blade and discharges radically into the atmosphere by the centrifugal action of the blades and the impeller. These types of fans handle smaller volumes of air at much higher pressure than axial fans (Howard 1997) as they compete for airflow.

2.4 Main Fan Components

A main fan usually consists of four components: impeller or rotor, motor and shaft, housing or casing, and evasée. A brief description of each of these components is presented below.

2.4.1 Impeller

This is the rotating part of the fan onto which the fan blades are mounted. The size of impeller determines the fan rating. If the speed of the fan is constant, the quantity of air handled by the fan is proportional to the square of the impeller diameter.

2.4.2 Motor and Shaft

The motor is the device that provides motion to the impeller through a shaft. It is driven either by fuel or electric power. The shaft transmits power from the fan motor to

the impeller.

The fan rating can also be controlled by changing the fan speed. This is usually done by changing the motor voltage through a variable speed drive or by changing the blade setting of the fan.

2.4.3 Housing

The fan housing provides protection to the fan. It includes an inlet duct on one side and one outlet on the other. In the case of a centrifugal fan, it resembles a scroll with one side an axial inlet and one a tangential outlet.

2.4.4 Evasée

This is an expansion cone attached to the fan outlet. It is used to recover part of the kinetic energy that otherwise would be lost to the atmosphere. Horizontal and vertical evasées are shown in Figure 2.5 and Figure 2.6, respectively.

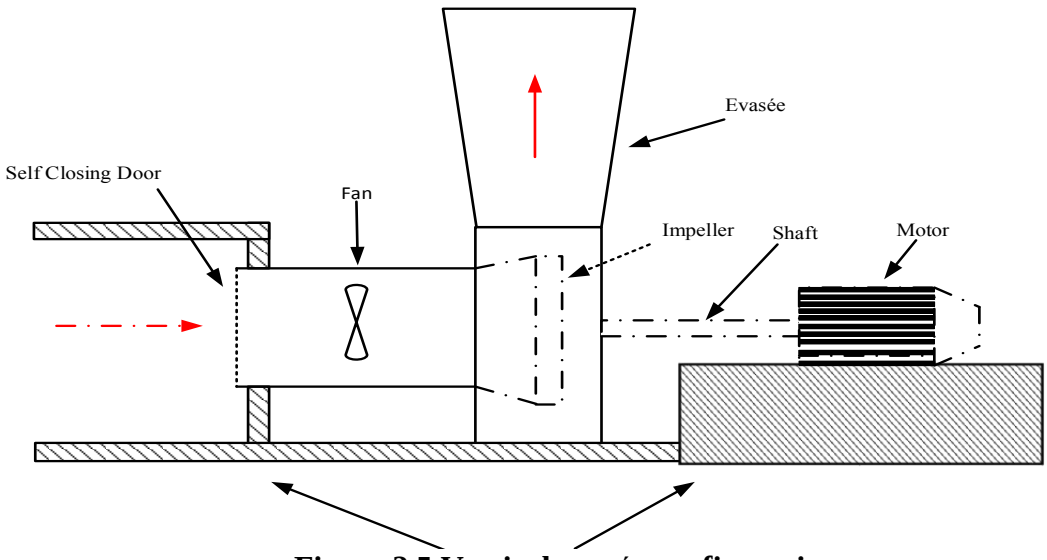

Figure 2.5 Vertical evasée configuration

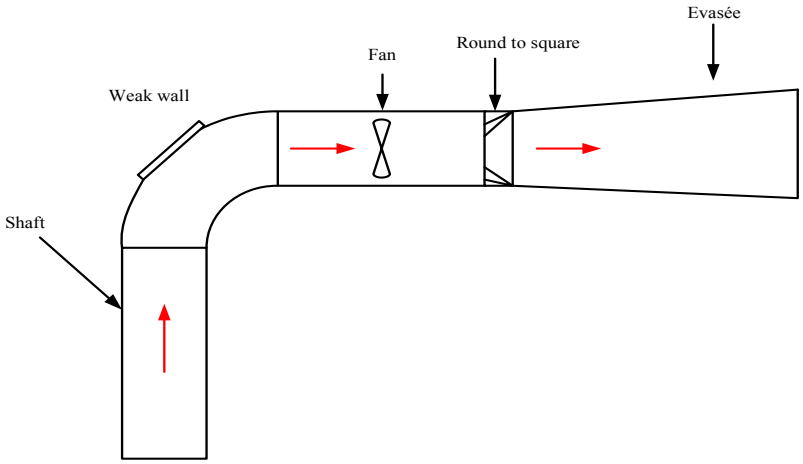

Figure 2.6 Horizontal evasée configuration

2.5 Fan Inlet Ductwork

As mentioned earlier, in designing the fan inlet duct, smooth transition of air direction is imperative. Turning vanes and a collar rollout can be used for this purpose. Refer to Figure 2.7 for details. Besides using turning vanes and shaft roll-out, another important factor is the length and diameter of the duct in-housing the fan. Refer to Chapter 5 for details.

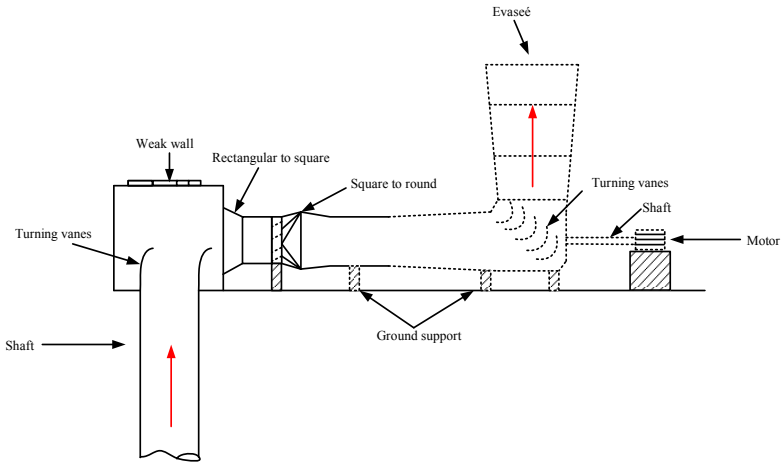

Figure 2.7 Fan inlet ductwork

2.6 Conclusion

In a typical fan installation for an underground coal mine, the air stream is subject to shock losses due to the turbulence. These shock losses can be minimized by using fan installation components. Some of these installation components include proper shaft collar design, incorporating turning vanes, and sufficient ductwork between the fan and the evaseé. Studies have shown that a proper design of the aforementioned components can significantly reduce the pressure losses. Also, by minimizing the pressure drop at the fan installation, these design components enable the fan to operate at a low total pressure and reduced the noise pollution level, which is considered to be a safety hazard.

CHAPTER 3

FAN SURVEY

With the increase in depth of an underground mine, the need for using high-pressure fans also increases. Fans used for ventilating mines are capable of moving large volumes of air. Maintaining smooth air flow patterns around the fan installations and mine openings is not simple since most of the air in the fan installation is in a turbulent state. It is not easy to take any measurement in turbulent regions because of the random nature of the turbulent. To ensure this smooth flow, reliable data must be obtained while performing fan surveys. This chapter discusses the major aspects of fan surveys: pressure, pressure head, and modified energy equation. A study of fan installation systems is also part of this chapter. The chapter ends with a fan survey conducted in an experimental mine. The purpose of discussing the fan survey conducted in an experimental mine is to determine the sources of the shock losses.

3.1 Pressure and Pressure Head

Physical quantities such as density, pressure, and temperature are essential are important for the description of the fluid mechanic processes. These terms are expressed in term of molecular quantities for ideal gases. For this chapter, pressure and pressure head are described in the following subheadings:

3.1.1 Pressure

Pressure is defined as the force exerted by fluid per unit area. Mathematically it is given as:

$$P = \frac{F}{A} \tag{3.1}$$

where

P = pressure (Pa)

F = force (N)

A = area (m^2)

3.1.2 Pressure Head

Pressure head is the pressure exerted by a column of water or other liquid that is equivalent to the pressure exerted by air. The pressure exerted by air is calculated by the following Equation:

$$P = \rho g h \tag{3.2}$$

where

ρ= density of air (kg/m^3)

g = acceleration due to gravity (m/s^2)

h = height of the liquid (m or mm)

Simplifying Equation 3.2

$$h = \frac{P}{\rho\, g} \tag{3.3}$$

A manometer, used to measure gauge pressure, is based on Equation 3.3. Figure 3.1 shows an inclined manometer. The pressure difference is calculated by measuring the

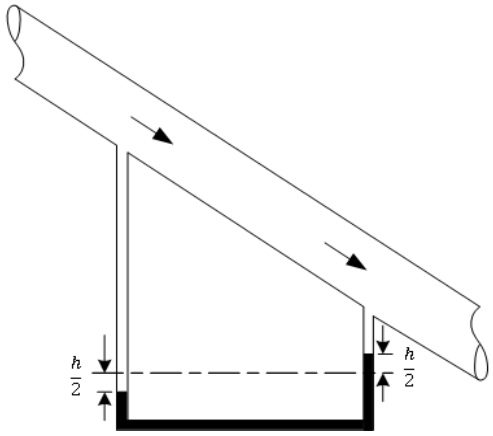

Figure 3.1 Inclined manometer

vertical difference of liquid levels as shown in Figure 3.1. This pressure difference is partly due to friction and partly due to gravity. This is further discussed in Section 3.2.

3.2 Modified Energy Equations

Modified energy equation is a variant of Bernoulli's equation. It is used for calculating the energy changes that take place in a fluid-flow system. The modified energy equation is given in Equation 3.4.

Total energy at section 1 = total energy at section 2 + energy losses due to flow

$$h_{s1} + h_{v1} + h_{z1} = h_{s2} + h_{v2} + h_{z2} + h_l \quad (3.4)$$

where

h_s = static head (m)

h_v = velocity head (m)

h_z = potential head (m)

h_l = energy loss due to friction and obstructions (m)

Since the change in elevation is small in a mine airway, gauge pressure heads can be used instead of absolute pressure head without sacrificing any accuracy. Thus

Equation 3.4 in terms of gauge pressure is given by:

$$h_{s1} + h_{v1} = h_{s2} + h_{v2} + h_l \quad (3.5)$$

3.3 Fan Installations

There are three possible fan installations for ventilating a mine: exhaust fan installation, blower fan installation, and booster fan installation. The use of each installation is subject to local restrictions and/or federal and state regulations. For example, for a gaseous coal mine, state regulations require the exhaust installation.

For a metal mine, the federal regulations do not restrict fan installations. In addition to federal regulation, the installation systems are governed by other factors, such as site constraint and type of main entrance to the mine. A brief description of these three types of the installation system is presented below.

3.3.1 Exhaust Fan Installation

In an exhaust fan installation, the air enters the mine through a portal or shaft, directed to the workings and exhausted to the atmosphere by a surface fan. Underground coal mines are ventilated by exhaust fan in the U.S.

3.3.2 Blower Fan Installation

In a blower system, the air is forced into the mine by means of a fan. In this system, the fan is located at the top of a downcast shaft or at the portal of an intake drift or ramp. A blower system is not recommended in gaseous mines.

3.3.3 Booster Fan Installation

A booster fan is installed in a main airway. It is always in series (pushing or pulling in the same direction that the main fan does) with the main surface fan. This fan is used to decrease the surface fan pressure and reduce leakage and power consumption. This system has characteristics of both exhaust and blower systems.

At present, booster fan are used in several countries, including the United Kingdom, Australia, New Zealand, and China. However, in the United States, the use of booster fans is limited to metal and nonmetal mines.

3.4 Fan Pressure Profile

Fan pressure profile is helpful in studying the pressure losses (both total and static) at different sections of the fan installation. They are a graphical representation of the Equation 3.4. Before describing a pressure profile, the following definitions need to be introduced: fan total pressure, fan velocity pressure, and fan static pressure.

3.4.1 Fan Total Pressure

Fan total pressure is the increase in air pressure due to conversion of electrical/mechanical energy into pressure energy that is added to the air. It is usually measured using a pitot-static tube and a manometer. Mathematically it is given as:

$$F_t = P_{t2} - P_{t1} \tag{3.6}$$

where

F_t = fan total pressure (Pa)

P_{t2} = total pressure at fan inlet (Pa)

P_{t1}= total pressure at fan outlet (Pa)

It should be noted that P_{t2} is the total pressure at the outlet of the fan duct whereas P_{t1} is the total pressure at the inlet of the fan duct.

3.4.2 Fan Static Pressure

Fan static pressure is the difference between the fan total pressure and fan velocity pressure. It is measured by using a pitot-static tube and manometer. It is measured by gauging the pressure difference between static pressure at the outlet and total pressure at the inlet of the fan. It is given by:

$$F_s = P_{s2} - P_{t1} \tag{3.7}$$

where

F_s = fan static pressure (Pa)

P_{s2} = static pressure at the outlet (Pa)

P_{t1} = total pressure at the inlet (Pa)

3.4.3 Fan Velocity Pressure

Fan velocity pressure is pressure is the average velocity pressure measured at the fan outlet. Fan velocity pressure are to determine the air flow rate inside the fan installations. Mathematically, it is given by the following equation:

$$F_v = P_{t2} - P_{s2} \tag{3.8}$$

where

F_v = fan velocity pressure (Pa)

P_{s2} = static pressure at fan outlet (Pa)

P_{t2} = total pressure at fan outlet (Pa)

3.4.4 Exhaust Fan Pressure Profiles

In an exhaust system (Figure 3.2 where the main fan is located at the outlet end), the static pressure starts with negative pressure, creating a suction effect. This means that the total pressure at the inlet is always equal to zero.

However, at the discharge end, the static pressure is zero since the air is discharged to the atmosphere. The total pressure at the outlet end is equal to the velocity pressure (refer to Figure 3.3 for the pressure profiles of the model). This means that the pressure at the outlet can be used to calculate the air quantity.

It should be noted that both total and static pressure decrease with an increase in the distance from the inlet. However, at the evasée, the static pressure increases and the velocity pressure decreases. This in turn increases the fan static pressure. Also, since the cross-section for the duct remains the same, there the velocity pressure does not change and remains constant.

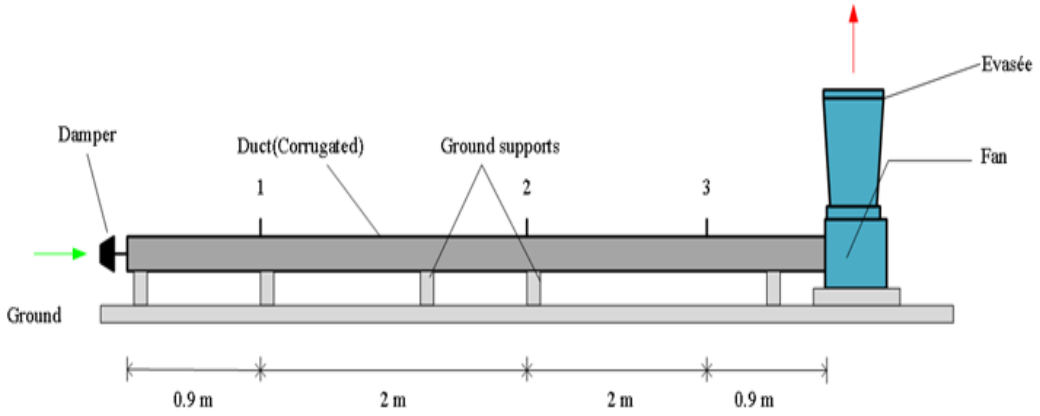

Figure 3.2 Exhaust fan installation model

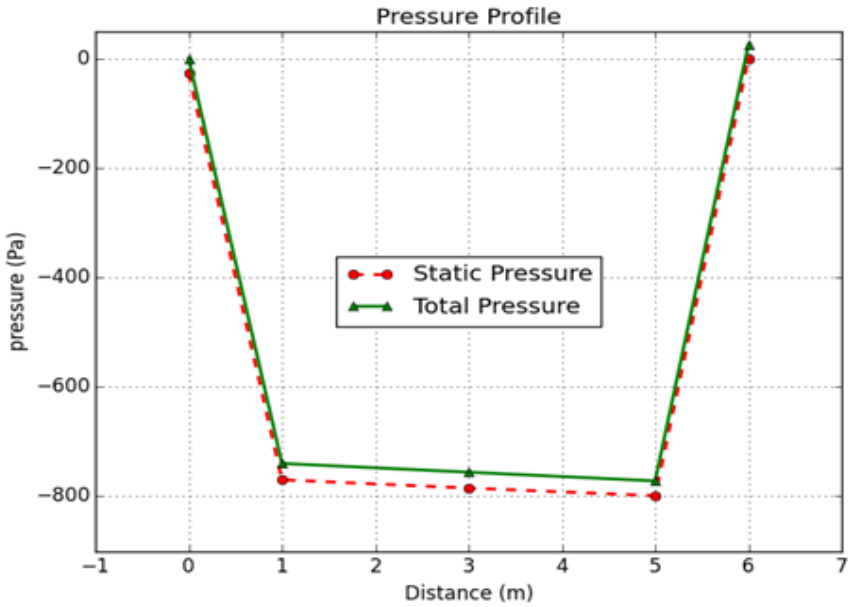

Figure 3.3 Pressure profiles for the exhaust model

3.5 Fan Survey at an Experimental Mine

The experimental mine uses an axial fan for ventilating the mine. It is installed as a blower fan near the top of a downcast shaft to which it is connected through a 12m long rigid duct and a 90° elbow. In addition, the mine is equipped with two booster fans. Figure 3.4 shows a schematic of the surface fan installation. As mentioned earlier in the chapter, the main purpose of this survey is to identify different shock loss factors in a fan installation.

First, all the physical dimensions of the fan installation components, such as fan diameter, fan duct length, radius of curvature for the elbow, etc. were measured. Then, the pressure generated by the fan was measured using a standard pitot-static tube and manometers. For shock losses in the system, they were calculated by finding shock loss factors.

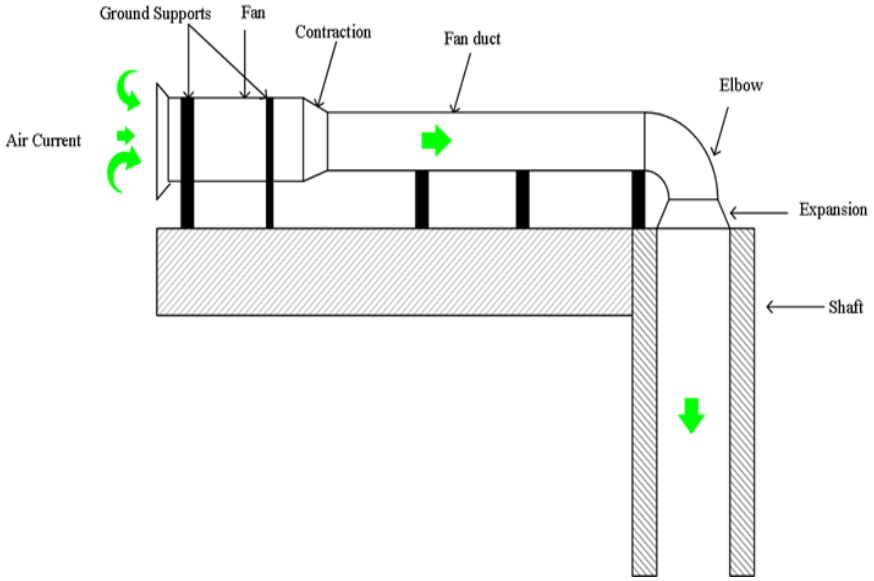

Figure 3.4 Schematic surface fan installation for the experimental mine

3.5.1 Fan Pressure Measurements

In mine ventilation, the main purpose of finding pressure drops is to determine the pressure difference due to the frictional and shock losses in the mine airway. There are two main methods to find the measure of pressure drops. The first method is known as the gauge and tube method. In this method, a gauge pressure between two stations is measured. The second method is known as barometric pressure survey. This method has several variations and depends on the pressure type being measured at the measuring station (McPherson 1993). In this survey, the first method is used for fan pressure. Gauge pressure was measured across the fan using a pitot-static tube.

However, as mentioned earlier, in order to measure a pressure drop across a mine shaft, two plastic tubes were inserted, one at the top and another at the bottom of the shaft. The other end of these plastic tubes was connected to a manometer. The gauge pressure reading was taken and recorded using a manometer as shown in Figure 3.5.

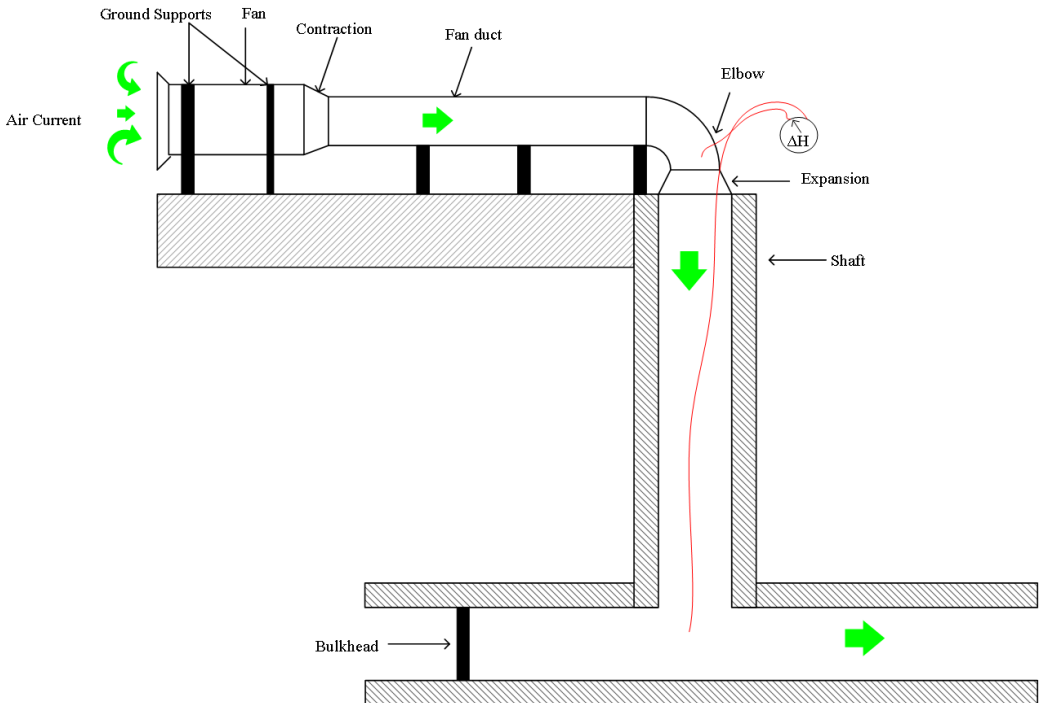

Figure 3.5 Pressure measurement at the shaft

3.5.2 Velocity Pressure Measurement

In order to calculate average air velocity in a duct, a set of velocity pressures is measured first, then the velocity is calculated. To measure the velocity pressure, the cross sectional area of the duct is divided into three concentric circles using Equation 3.9.

$$R_i = r \times \sqrt{\frac{2i - 1}{2\,N}} \tag{3.9}$$

where

r = radius of the duct (m)

R_i = radii from the center of the duct to the measuring station (m)

i = variable used to identify a measuring station

N = number of readings along the diameter (for example N = 6)

In Figure 3.6, R_i is the radii of the measuring stations. For a 1-m- diameter duct, the radii of the three concentric circles are 0.22 m, 0.38 m, and 0.49 m, respectively. One of the advantages of dividing the cross-sectional area into different sections is that average air quantity can be calculated in the duct.

For a given velocity pressure, p_v, the velocity of the air is calculated using Equation 3.10.

$$v = \sqrt{\frac{p_v \times 2}{\rho}} \tag{3.10}$$

where

ρ = density of fluid (kg/m^3)

v = velocity of air (m/s)

p_v = velocity pressure (Pa)

Using Equation 3.10, the air velocity is calculated for each of the radii and then the average velocity is determined by taking the arithmetic mean of the velocities. The average velocity in the fan duct was found to be 15.6 m/s. Based on this velocity, the flow rate was estimated at 14 m^3/s. The detail of flowrate is given in Section 3.5.3.

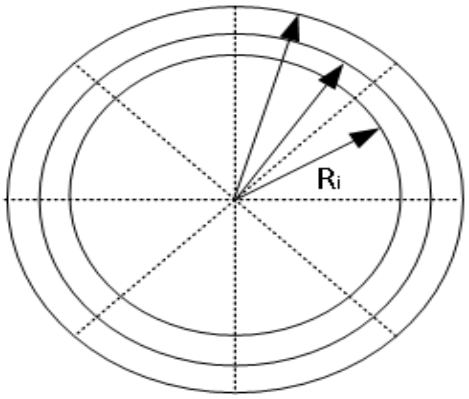

Figure 3.6 Division of circular cross-section into concentric circles

3.5.3 Measuring Flow Rate

Air volume flow rate can be calculated by measuring the air velocity in a fixed point in an airway using anemometer and average area at that given point.

$$Q = V \times A \tag{3.11}$$

where

Q = air quantity (m^3/s)

V= velocity of air (m/s) and

A = area of the duct (m^2)

Table 3.1 gives the fan detail of the fan power and its operating point. For this experimental mine, the fan is operating at a pressure of 1140 Pa and the air quantity for this given pressure is 14.13 m^3/s. The cross-sectional area of the fan is about 0.89 m^2 (refer to the Table 3.1 for details).

Table 3.1 Fan operating point and flow rate

Parameters	Values
Fan outlet duct diameter	1.07 m
Cross-sectional area	0.89 m^2
Fan motor power	22 k-W
Fan operating pressure	1140 Pa
Fan air quantity	14.15 m^3/s
Fan velocity	16 m/s
Fan velocity pressure	150 Pa
Fan total pressure	1290 Pa

3.5.4 Pressure Losses and Resistance Calculation

The fan used at the experimental mine is an axial type. This fan installation consists of a circular duct, and a 12 m long rectangular duct is used to connect the fan to the shaft collar. A 90° elbow between the fan and shaft is also part of this installation component. It connects the rectangular duct to the shaft (refer to Figure 3.5). The final installation component is a sharp expansion at the shaft collar.

The resistance of each component is calculated separately and then added to get the equivalent resistance. The resistances are calculated using Atkinson's equation, given in Equation 3.12.

$$R = k \times per \times L/A^3 \tag{3.12}$$

where

R = resistance (N s^2/m^8)

k = friction factor (kg/m^3)

per = wetting perimeter of the duct (m)

L= length of duct (m)

A = area of the duct (m^2)

First, the resistance of the circular duct, R_1, is calculated using Equation 3.7. The area of this circular duct is 0.893 m^2. A friction factor of 0.00463 kg/m^3 (smooth duct) is used for this segment. The resistance, R_1, is given as:

$$R_1 = 0.1844 \quad Ns^2/m^8$$

After calculating the resistance of the circular duct, the resistance due to contraction is calculated using empirical formula. This contraction is due to the transition from circular to square as shown in Figure 3.5. The shock loss factor, X, as a result of this contraction can be calculated by measuring the area of the circular duct and rectangular

duct and using Equation 3.13.

$$X = \left[\frac{A_2}{A_1} - 1\right]^2 \tag{3.13}$$

where

X = shock loss factor

A_1 and A_2= areas at the inlet and outlet of the contraction respectively (m^2)

The value of A_1 andA_2 are 0.89 m^2 and 1.03 m^2, respectively. The value of X using 3.8 is 0.024. Now that the shock loss factor is known, the value of resistance, R_2, as a result of this contraction is determined by using Equation 3.14.

$$R_{shock} = X \times \frac{\rho}{2A^2} \tag{3.14}$$

where

ρ = density of air (kg/m^3)

$$R_2 = 0.0162\ Ns^2/m^8$$

Resistance of a square conduct connecting the fan to the shaft collar is denoted by R_3. This resistance is calculated using Equation 3.13. The value of this resistance is given below:

$$R_3 = 0.05254\ \frac{Ns^2}{m^8}$$

As shown in Figure 3.5, the fan is conducted to the shaft through a 90° elbow. The dimension of the elbow is given in Figure 3.7. In order to calculate the resistance, R_4, of the elbow, first the shock loss factor, X, is calculated using Equation 3.15.

$$X = \frac{0.25}{m^2 \times \sqrt{a}} \tag{3.15}$$

where

m = ratio of radius of curvature to the width of the duct

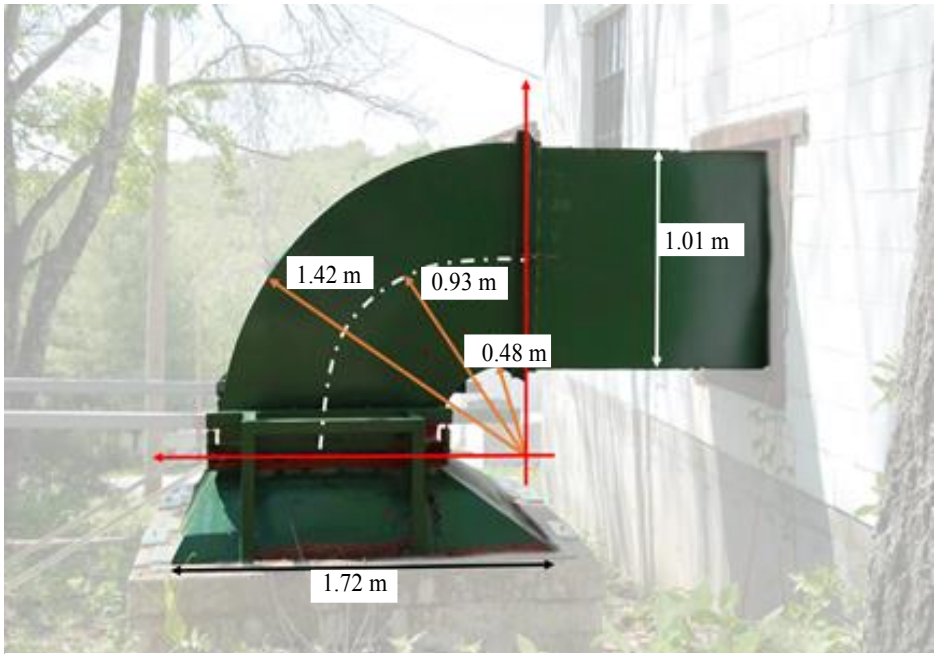

Figure 3.7 Dimensions of the elbow

a = aspect ratio height/width

X = shock loss factor

Using Equation 3.15 and Equation 3.14, the value of R_4 is calculated and is given below:

$$R_4 = 0.164 \frac{Ns^2}{m^8}$$

The sudden expansion between the below and the shaft collar causes shock loss. This shock loss can be determined using Equation 3.13. The resistance of the sudden expansion, R_5, can be calculated using Equation 3.14. The value of R_5 is given below:

$$R_5 = 2.0068 \frac{Ns^2}{m^8}$$

Total resistance for this fan installation is calculated by adding all the resistances. Since all the resistances series were calculated. The total resistance, R_T, is using Equation 3.16.

$$R_T = R_1 + R_2 + R_3 + R_4 + R_5 \quad (3.16)$$

The total resistance R_T calculated is given below.

$$R_T = 2.423\ Ns^2/m^8$$

3.6 Conclusion

Atkinson's equation shows that the resistance remains constant for any given air path unless there is a major change in it. The resistance of an airway, in addition to its physical dimensions, depends on the friction factor. The value of k itself varies with the density of the air. It follows that resistance depends on the density. The resistance due to friction is smaller than that of resistance due to shock losses. This is due to a change in the direction of the airflow or air velocity, as additional vortices are generated which in turn change the resistance of the airway. The propagation of these vortices creates eddies which may increase the airway resistance significantly.

In general, the resistance of an airway can be represented by the following equation:

$$R_{equivalent} = R_{friction} + R_{shock} \quad (3.17)$$

Decreasing the value of the resistance due to shock losses will increase the quantity of air. This can be explained by considering the equation given below:

$$F_t = F_s + F_v \quad (3.18)$$

Since the total fan pressure remains constant, by eliminating shock losses by removing any obstructions and bends (shock losses), the static pressure (of the fan) will decrease and this in turn will increase the velocity pressure. An increase in velocity pressure means increasing the quantity of the air.

In an exhaust system, the way the fan is attached to the fan house (or shaft collar) determines to great extent the success or failure of the ventilation system. Similarly, in a blower system, the way the fan is attached to the intake portal plays an important role. Therefore, to get the best of a main fan, it is crucial to have an adequate design, proper installation, and well-established fan maintenance and operating procedures. Keeping the fan house clear of any obstructions and monitoring the fan inlet and outlet ducts for any leakage will improve fan performance.

CHAPTER 4

RESEARCH METHODOLOGY

This chapter presents an introduction to Computational Fluid Dynamics (CFD), its basic working principals, the modeling of a sample problem, a venturi-tube, and a summary of results. The results of these simulation runs were validated using pressure quantity measurements collected from a physical model.

4.1 Introduction to CFD

In the early 1980s, CFD had limited applications and was reduced to simulation studies in aeronautics and astronautics. In the 1990s, due to rapid changes in computer technology, both in the hardware and software, CFD gradually became an integral part of many industries that involve fluid flow. Currently, CFD is a new branch of engineering sciences that integrates three discipline of science: fluid dynamics, mathematics, and computer science as shown in Figure 4.1(Jiyuan et al. 2008).

Fluid dynamics is essentially the study of fluid flow under laminar or turbulent flow conditions. It also includes the study of heat transfer. The behavior of the fluid mechanics are described through mathematical equations based on Kirchhoff's laws, and conservation of mass, energy, and momentum. The knowledge of these basic concepts is needed to formulate and run CFD models and interpret the different results.

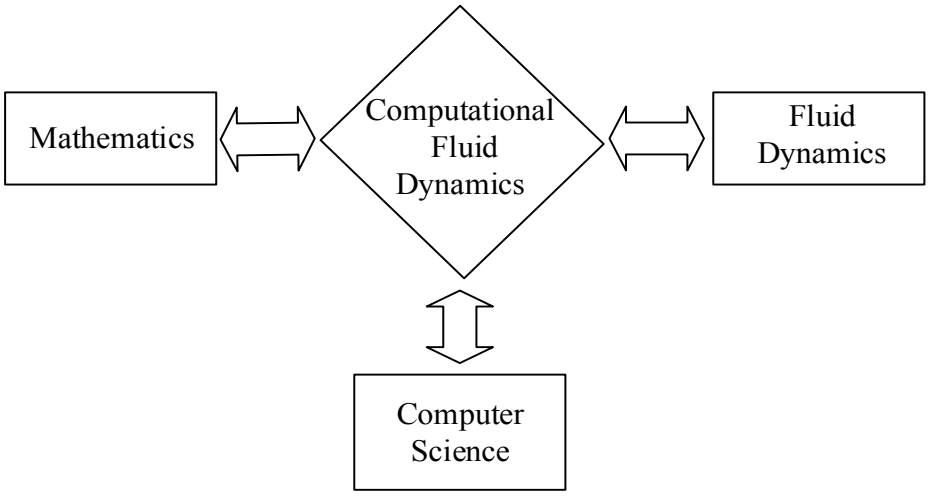

Figure 4.1 Different disciplines integrated with CFD

4.2 Application of CFD in Mining Engineering

In today's world, there is a huge demand for natural energy resources such as water, natural gas, oil, and coal. In order to quench the thirst for these resources in both developed and underdeveloped countries, underground mines have been turned into underground cities. This means that mine ventilation is defined as a science of not only supplying sufficient quantities of air through mine openings, but maintaining good standards of air quality. The responsibility of today's mine ventilation engineers is to meet these objectives effectively and efficiently. This has geared mining engineers towards producing economic designs using the best technology available in all aspects spanning from shaft sinking and developing aerodynamic airways, to proper installation of air moving devices such as fans, compressors, etc.

Changes in fluid flow phenomenon such as the rise in air pressure, changes in temperature, and density of air have sparked a lot of research work in mine ventilation utilizing CFD.

4.3 Basic Governing Equations Used in CFD

CFD works on a set of basic governing equations. These are often called the conservation laws of physics. These equations are based on the following assumptions:

1. Conservation of mass
2. Conservation of momentum and energy
3. Conversation of thermal energy

The principals of each law are discussed below.

4.3.1 Conservation of Mass

The principle as applied to mine ventilation can be stated as follows: the mass flow rate passing along any cross-section of an airway is constant provided that the flow is in steady state condition and there is no inflow or outflow of the fluid between two sections of the airway. Mathematically it is given as:

$$m_{in} - m_{out} = 0 \tag{4.1}$$

where

m_{in} = mass flow rate (kg/s)

m_{out} = mass flowrate (kg/s)

Mathematically, mass flow rate and volume flow rate are related by:

$$m = \rho \times Q \tag{4.2}$$

where

ρ = density of air (kg/m^3)

Q = volume flowrate (m^3/s)

In mine ventilation, most flow quantity measurements are based on volume flowrates. From Equation 4.1 and Equation 4.2.

$$(\rho V A)_{in} = (\rho V A)_{out} \quad (4.3)$$

In most mines, the air density is fairly constant, especially in single level mines. Hence Equation 4.3 can be written as:

$$Q_{in} = Q_{out} \quad (4.4)$$

Continuity equations such as 4.4 and 4.3 hold for most fluid flow except for slip conditions. In simple words, if the fluid does not stick to the boundaries of the model, then total mass of fluid entering the system is equal to the total mass leaving the system.

4.3.2 Conservation of Momentum and Energy

The Navier-Stokes equation describes the momentum of a moving fluid in terms of velocity, pressure, temperature, and density. The study of the Navier- Stokes equation is beyond the scope of this work. However, a brief discussion of the Bernoulli's equation for energy is discussed below:

For inviscid flow, the Bernoulli's equation is given by:

$$\frac{p}{\rho} + \frac{V^2}{2} + gz = \text{constant} \quad (4.5)$$

where

p = pressure (Pa)

ρ = density of fluid (kg/m^3)

g = acceleration due to gravity (m/s^2)

z = elevation above or below the datum line

v = velocity of the fluid (m/s)

The above equation is often written between two sections of fluid flow inside a duct or airway (refer to Figure 4.2).

$$\frac{p_1}{\rho} + \frac{V_1^2}{2} + gz_1 = \frac{p_2}{\rho} + \frac{V_2^2}{2} + gz_2 \tag{4.6}$$

Dividing by g, Equation 4.6 gives an expression in terms of head

$$\frac{p_1}{\gamma} + \frac{V_1^2}{\gamma} + z_1 = \frac{p_2}{\gamma} + \frac{V_2^2}{\gamma} + z_2 \tag{4.7}$$

where

γ = specific weight of the fluid (N/m^3) = ρgh

p = pressure (Pa)

ρ = density of fluid (kg/m^3)

g = acceleration due to gravity (m/s^2)

z = elevation above or below the datum line

v = velocity of the fluid (m/s)

Figure 4.2 Two different sections of venturi-tube

4.3.3 Conservation of Thermal Energy

For a fluid in motion, the conservation of thermal energy refers to changes in the internal energy due to the microscopic and macroscopic motion of the fluid. The first law of thermodynamics basically states that energy cannot be created or destroyed in an isolated system. It changes from one form into another form of energy. Mathematically, the first law of thermodynamics can be expressed as:

$$E = Q + W \tag{4.8}$$

where

E = total energy of the system (J)

Q = heat transfer of the system (J), it is positive when heat is added to the system from the surrounding.

W = work done (J), it is positive when work is done by the system.

The second law of thermodynamics deals with the entropy of a system. For an irreversible thermal process, the change in the entropy for a system is always positive. Mathematically, the second law of thermodynamics can be expressed as:

$$S = S_f - S_i = \frac{Q}{T}$$

where

S = change in entropy of the system (J/K)

S_f = final entropy of the system (J/K)

S_i = initial entropy of the system (J/K)

Q = heat added to the system (J). It is positive when heat is added to the system and negative when heat is removed from the system.

T = absolute temperature of air in the system (K)

This research work does not involve any change in the thermodynamic properties of the air since the density and temperature of the air remain practically constant at the fan installation. Therefore, the thermal energy equation option (In ANSYS FLUENT) was suppressed when solving for the governing equations.

4.4 Simulation Exercise – Venturi-tube

A physical experiment on a venturi-tube was conducted at the University of Utah ventilation laboratory. The purpose of the experiment was to collect field data on pressure drop in a venturi-tube. The venturi-tube is connected to a blower fan as shown in Figure 4.3. Pressure heads were tested at station 1, 2, 3, and 4. These pressure readings were then used to calibrate a CFD model.

In order to simulate the air flow through a venturi-tube, a 3-D model was created using ANSYS software. Figure 4.4 shows a 3-D geometry of the venturi tube. Surface features such as hinges and pressure tabs of the model were eliminated while creating the model.

In this numerical analysis, the outlet and inlet ducts were extend far enough (15 times diameter) to counter the reverse flow at the inlet and outlet. In most of simulation works, it is common practice to extend far enough to counter the reverse flow at the outlet.

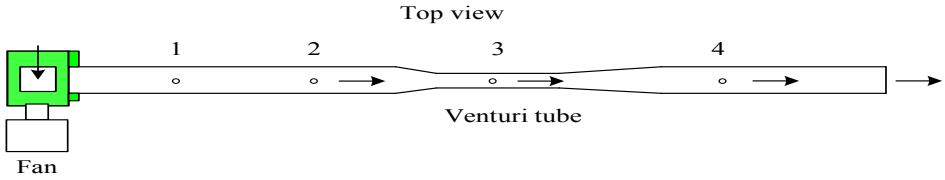

Figure 4.3 Venturi-tube laboratory model

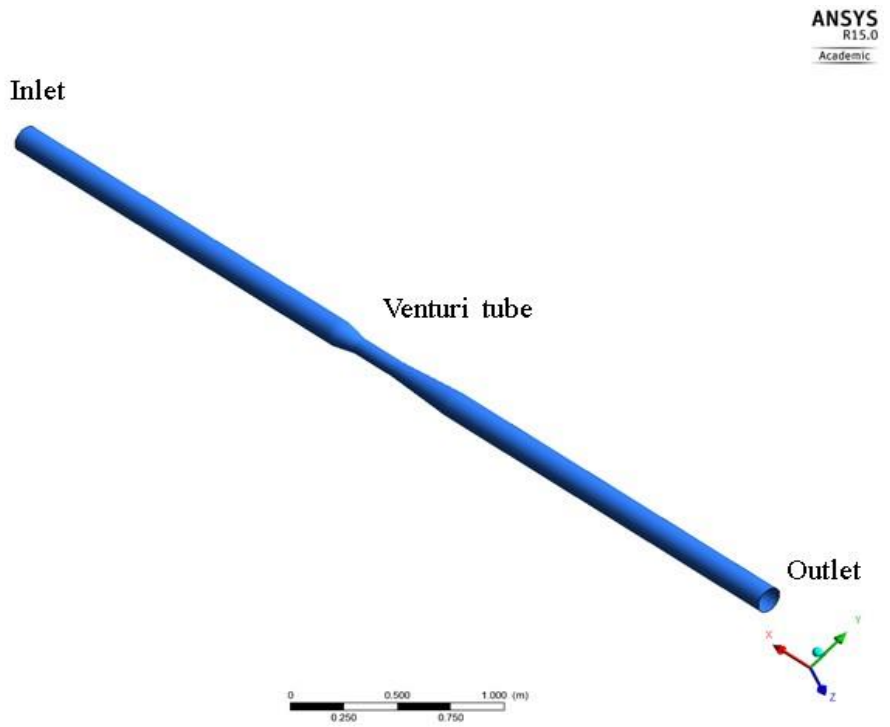

Figure 4.4 Geometry of the venturi-tube

Table 4.1 gives the dimensions of the venturi-tube. The inlet angle, $\Theta_{inlet,}$ is the angle at the inlet of the venturi-tube whereas outlet angle, Θ_{outlet}, is the angle at the outlet of the venturi-tube.

Once the model is meshed and the boundary conditions are specified, CFD is used to solve the fluid flow problem for flow patterns and pressure contours. For meshing the model, the body of model is divided into small volumes by generating smaller grids within the fluid domains. Then the governing equations are solved for each finite volume.

Figure 4.5 shows the surface mesh of the model. Structured mesh is used for the entire fluid domain. Boundary layers (prism grids) were generated at the walls of the model. These boundary layers capture the detail of the viscous flow that is dominant at the boundaries of the model.

Table 4.1 Dimensions of venturi-tube

Parameter	Dimensions
Diameter	0.138 m
Total length	16 m
Venturi-diameter	0.08 m
Venturi- length	0.254 m
Θ_{inlet}	11.57 °
Θ_{outlet}	4°

Figure 4.5 Surface mesh of venturi-tube

The governing equations in CFD are solved by assigning initial boundary conditions which in this case are represented by pressure at the inlet and outlet. These boundary conditions convert the governing equations into a set of algebraic equations. Table 4.2 summarizes the measured quantities used in the modeling exercise.

In CFD analysis, the simulation results must meet a desired level of accuracy. In order to meet this level of accuracy, different physical quantities (mass, velocity, momentum, k, epsilon etc.) are monitored after each iteration.

Table 4.2 Physical quantities measured

Parameter	Measurements
Barometric Pressure	8.6e4 Pa
Air Density	1 kg/m^3
Temperature	24 ° C
Dynamic Viscosity	1.8e-5 kg/m-s
Reynolds Number	1.4e5
Quantity of Air	0.27 m^3/s
Average Velocity	18.23 m/s
Static pressure at station 1	548 Pa
Static pressure at station 2	498 Pa
Static pressure at station 3	-287 Pa
Static pressure at station 4	398 Pa
Static pressure at outlet	320 Pa

If all the modeling parameters (for example, boundary conditions, turbulence model, mesh quality) are specified correctly during formulation, then the imbalance (known as residuals) in these physical quantities are lowered after each iteration.

In this simulation work for the venturi-tube, the residuals were monitored continuously. The iterations stopped once the desired level of accuracy specified were achieved. Figure 4.6 shows the residuals values after each iteration.

Once the solution is converged to the desire level as explained above, the simulation results were analyzed using the postprocessing toolbox of ANSYS software. The pressure gradients for the venturi-tube were studied first using the toolbox.

Figure 4.7 shows the pressure profiles of the venturi-tube. The total pressure decreases in the direction of the flow. The static pressure gradient clearly shows the conversion of static pressure into velocity pressure in the venturi-tube and partial

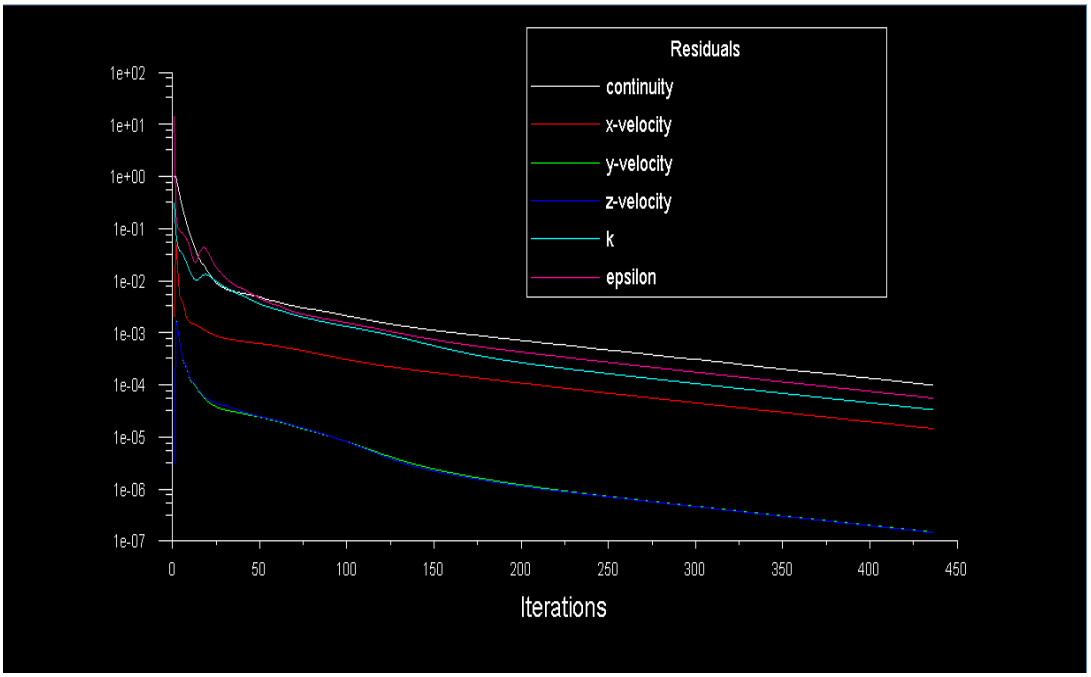

Figure 4.6 Value of residuals after each iteration

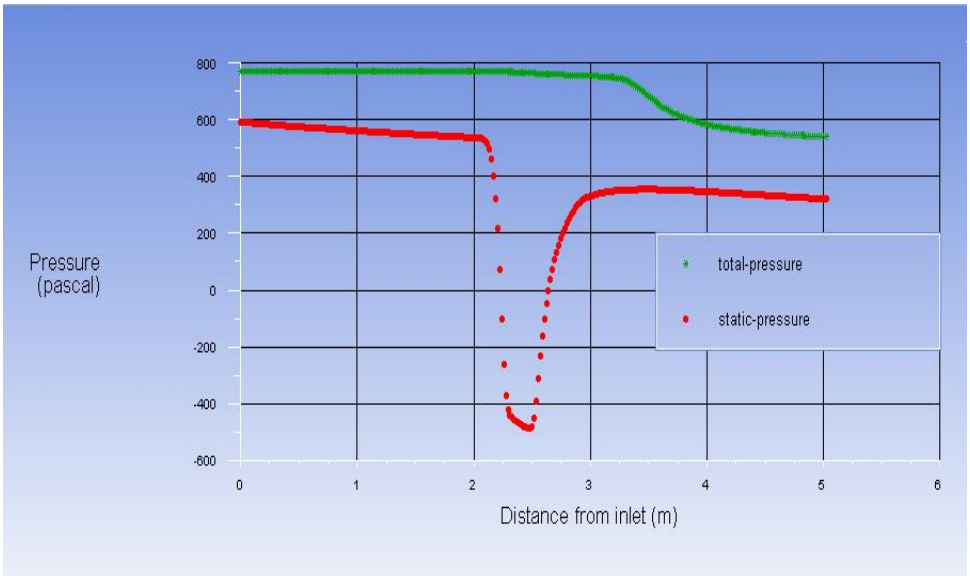

Figure 4.7 Pressure profile for the venturi-tube

conversion of velocity pressure into static pressure at the end of the venturi-tube. The sudden pressure drop at the entrance of the tube and the pressure build up at the end of the discharge illustrate the changes in velocity pressure due to changes in cross-sections of the model.

In a manner similar to pressure profiles, velocity contours were also analyzed for this exercise. In order to analyze these contours, the model was sliced into two equal halves and a plane is created in the middle of the model. Velocity contours were generated in the middle plane. Figure 4.8 shows the velocity contours for the model.

From these velocity contours (refer to Figure 4.8), it is clear that the magnitude of the air velocity reaches its maximum at the throat of the venturi-tube. This is due to the smaller cross-sectional area of the venturi-tube.

Table 4.3 shows a comparison of results between the physical model and numerical model for the standard mesh setting. The results of quantities measured in the numerical model are not mesh dependent.

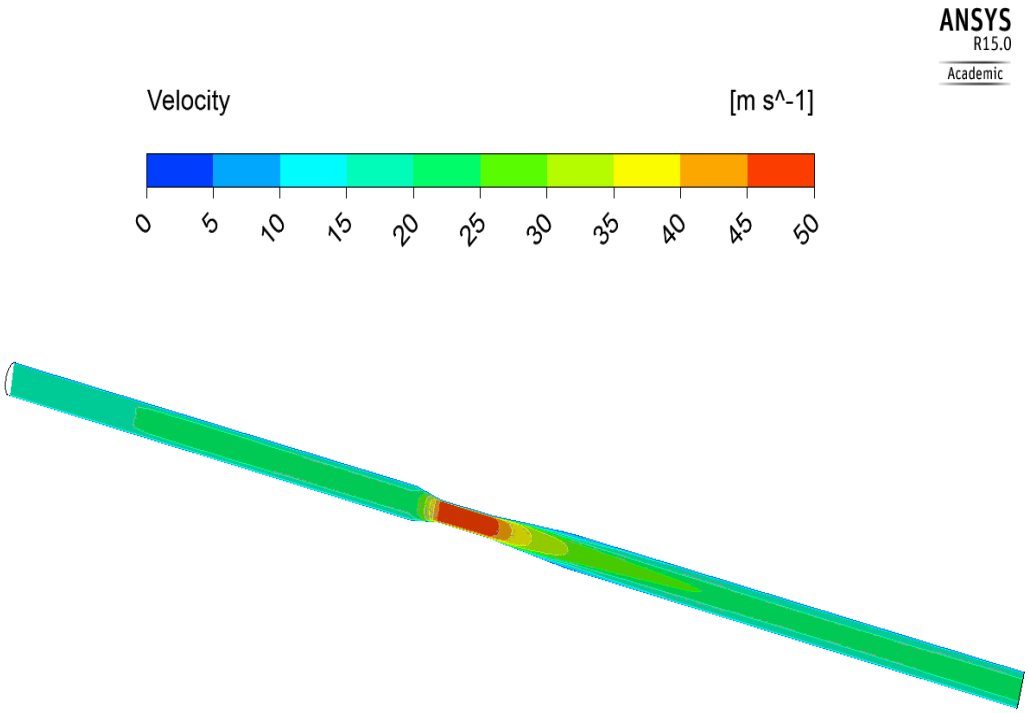

Figure 4.8 Velocity contours for venturi-tube

Table 4.3 Comparison between physical and numerical model

Parameters	Physical Model	Numerical Model
Volume flowrate	0.27 m^3/s	0.28 m^3/s
Velocity inlet	18.23 m/s	19 m/s
Static pressure at inlet	605 Pa	605 Pa
Static pressure at 1	548 Pa	548 Pa
Static pressure at 2	498 Pa	523 Pa
Static pressure at 3	-287 Pa	-411 Pa
Static pressure at 4	398 Pa	340 Pa
Static pressure at outlet	320 Pa	320 Pa

4.5 Conclusion

This chapter demonstrates the application of a numerical model by explaining the basic principles of CFD and simulating a laboratory model using ANSYS, FLUENT. The parameters measured in the laboratory were used to determine the boundary conditions of the numerical model. Then the results of the CFD model were compared with those collected from the physical model. Except for the venturi-tube section, the results compared very well. The only drawback of this analysis is that the grid- independent studies were not performed during CFD modeling. These studies could have improved the quality of the results by including the friction factor calculation in the venturi-tube section. The aim of this work is to determine relative changes in pressure in an airway due to obstruction rather than absolute values. Therefore, a mesh-independency test is not required for the modeling exercises performed in this study.

CHAPTER 5

MINE A: BLOWER SYSTEM

This study researches the pressure losses and air behavior in a fan installation. Two fan installation systems—a blower system and an exhaust system for an underground mine— are studied for this purpose. A blower system is discussed in this chapter and an exhaust system in Chapter 6. Using Computation Fluid Dynamics software, the blower system model was simulated. The analysis of data obtained from these simulations showed a significant pressure loss at different sections of the fan installation system. These pressure losses were mainly due to shock losses. The sources of some of these losses were identified and evaluated. As a result of this research, it was found that increasing the length of the fan diffuser and avoiding the right angle turns could recover part of these pressure losses.

5.1 Geometry of Blower System

Figure 5.1 shows the geometry for the blower system. The installation components for this system mainly consist of an inlet cone, an axial fan, and an outlet duct which is followed by a right angle turn. It should be noted that Figure 5.1 is a schematic of the blower fan system. The details of each of these components are given in Table 5.1.

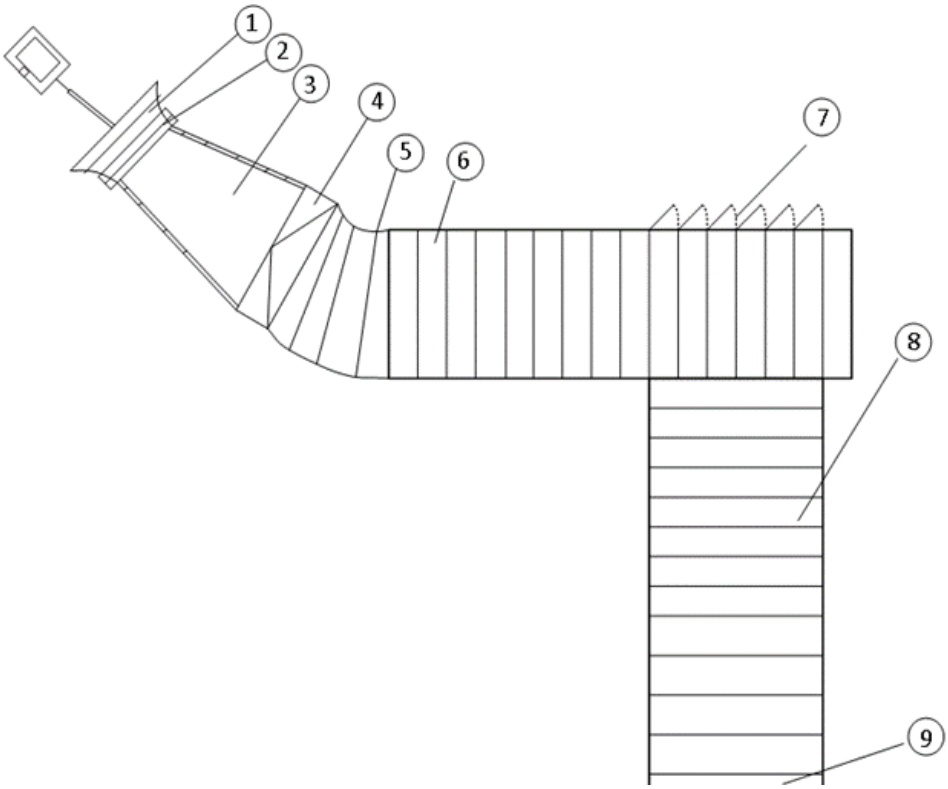

Figure 5.1 Schematic fan installation diagram

Table 5.1 Fan installation components

Parts/Components	Description
Number 1	Fan inlet cone
Number 2	Fan
Number 3	Fan diffuser
Number 4	Round to square transition
Number 5	Duct with acute angle turn
Number 6	Straight duct
Number 7	Weak wall
Number 8	Duct elbow
Number 9	Outlet

A simplified 3-D model of the blower system (see Figure 5.1) is generated using Design Modeler[1] and is shown in Figure 5.2. The model was generated without surface features such as the corrugated inner surface. This is done to save computational memory and simulation time. These kind of surface features are not generated in simulation work because they add resistance to the flow and do not affect the flow behavior. The resistance of the wall in the model is a function of wall roughness (y-plus value). The y-plus value is a function of the mesh size and not a function of surface features.

Refer to Table 5.2 for the dimension of the installation for the blower system. The dimensions of the component are arbitrary and based on typical fan installation sizes in the U.S. This installation will be referred to as a base case. All the parametric studies will be compared with the base case.

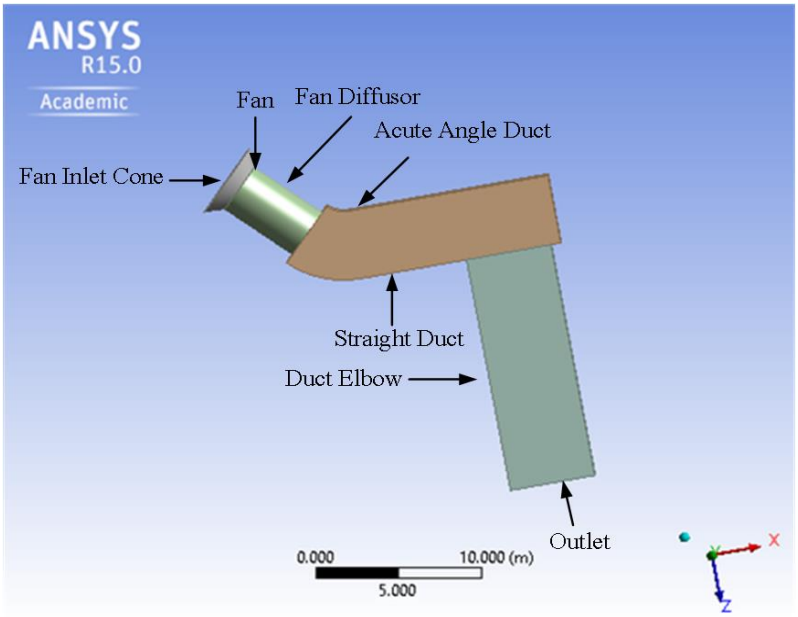

Figure 5.2 Geometry of the blower system

[1] Design Modeler is a CAD software, developed by ASYS.

Table 5.2 Dimension for the geometry of blower system

Description	Dimension
Fan inlet cone	Diameter = 4.8 m
Fan diffuser	Length = 6.0 m, Diameter = 3 m
Duct with acute angle	Total Length = 5.0 m Height = 4 m and Width = 4 m
Straight duct	Length = 6.4 m Height = 4 m and Width = 4 m
Elbow duct	Length = 8.0 m Height = 4 m and Width = 4 m
Outlet	Width = 5.2 m and Height = 4 m

5.2 Mesh Generation

In order to simulate the flow distribution and pressure losses in the model, the flow domain is divided into smaller grids. These grids are also known as meshes. Figure 5.3 is an example of a 2-D flow domain with a quadrilateral mesh. The fluid enters the fluid domain at the inlet (in this case a duct) and leaves it at the outlet.

Mesh is generated in order to predict the flow behavior within the fluid domain by solving the governing equations for each of the grids. However, there are a number of factors that are important that need to be taken into consideration before generating mesh.

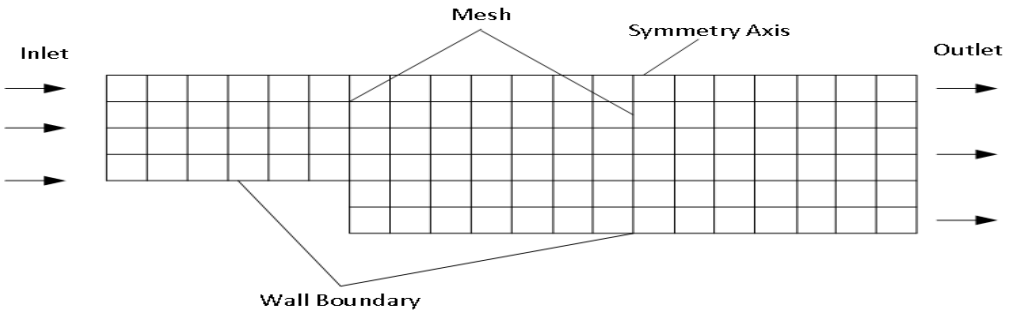

Figure 5.3 Sketch of a quadrilateral mesh in 2D

Mesh sizes, mesh structure, mesh quality, y plus values, and contact regions are some of these important factors. Explaining these factors is beyond the scope of this work. However, the reason for mentioning it here is to emphasize the importance of these factors. If any of these factors are neglected, the solution of the flow problem will not converge or does not give an accurate result (Jiyuan Tu 2008).

Figure 5.4 shows the mesh generated for the blower model. A default 3-D unstructured mesh is generated in the fluid domain. The flow at the boundary of the wall requires proper resolution of the grids to capture boundary details. Therefore, the boundary layer (also known as inflation layers) is generated near the wall of the model. The boundary layer is made of a structured prism mesh (see Figure 5.4).

5.3 Numerical Simulation

Based on the assumptions discussed in Chapter 4, the simulation parameters for this model are given Table 5.3. In this research, mostly default settings for material properties were used for simplicity. A standard k-ε turbulence model was used for flow prediction.

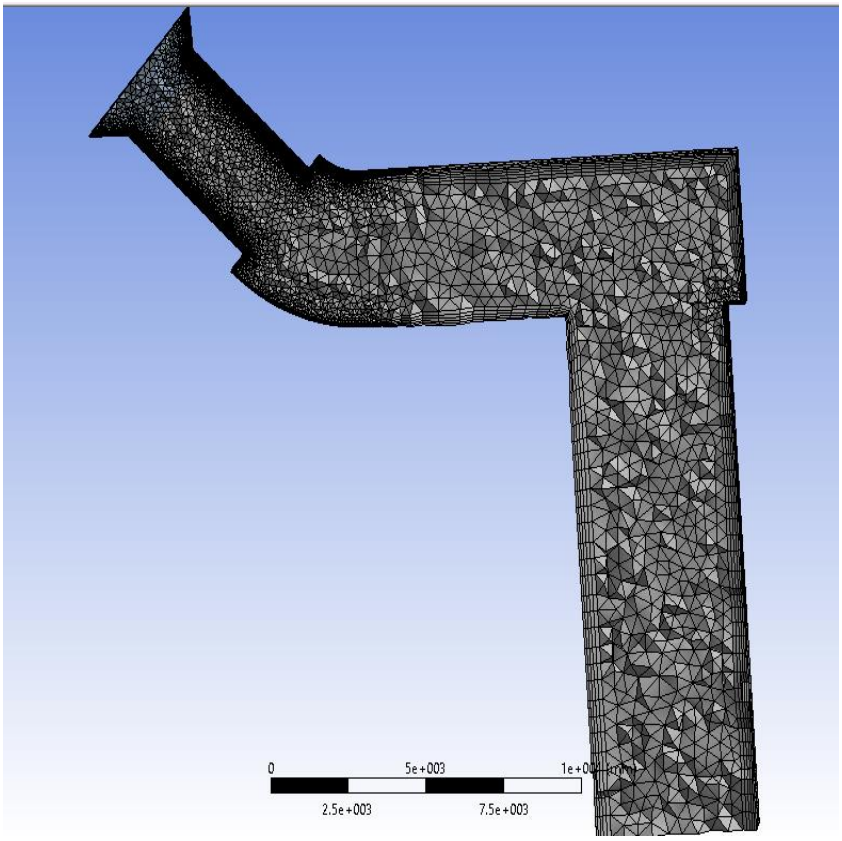

Figure 5.4 Mesh generation for the base case

Table 5.3 Simulation parameters

Parameters	Input Values
Turbulence model	k-ε model
Wall treatment	Enhanced wall treatment
Boundary conditions	Velocity inlet, fan, pressure outlet
Material properties	Density = 1.225 kg/m^3
	Viscosity = 2e-05 kg/m-s
Initialization method	Standard inlet initialization

For this reason, enhanced wall treatment was activated to capture the detail of this viscous flow at the walls of the installation. With a good quality mesh, the k- ε turbulence model along with enhanced wall treatment worked best for most of the fan installation models. The solution converges a reasonable number of iterations.

The physical quantities such as mass, momentum, and k-epsilon are selected to check for the convergence of the solution (see Figure 5.5). For this simulation, the solution converged to the desired level of accuracy after almost 200 iterations.

The boundary conditions for the inlet, outlet, and fan are shown in Figure 5.6. The air quantity is determined by using the fan intake boundary condition. It should be noted that due to limited computational memory, a moderate fan pressure of 700 Pa was used for simulation.

This fan pressure converges without performing too many iterations. However, for the postprocessing of the results, instead of fan intake, a second simulation is performed. In the second simulation, velocity magnitude (determined in first simulation) was assigned at the inlet (see Figure 5.6).

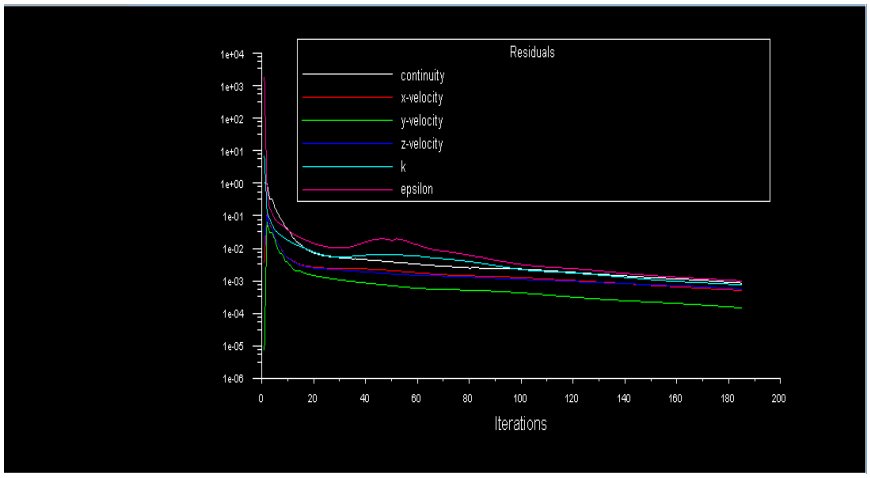

Figure 5.5 Residual plot for the base case

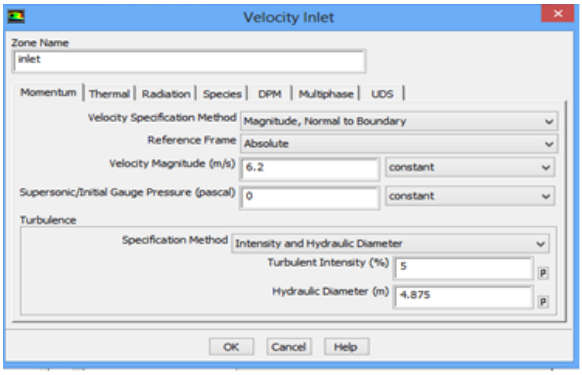

Inlet boundary Condition

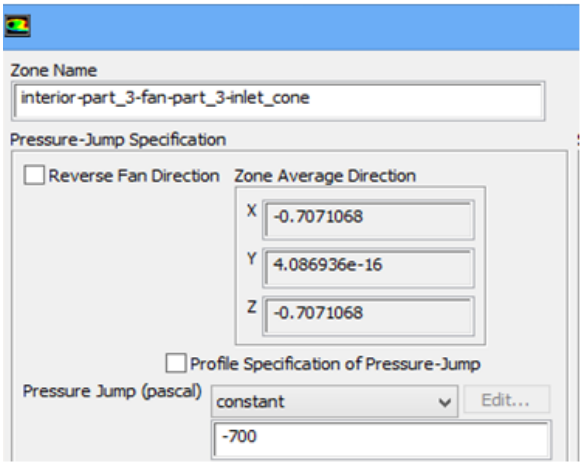

Fan Boundary Condition

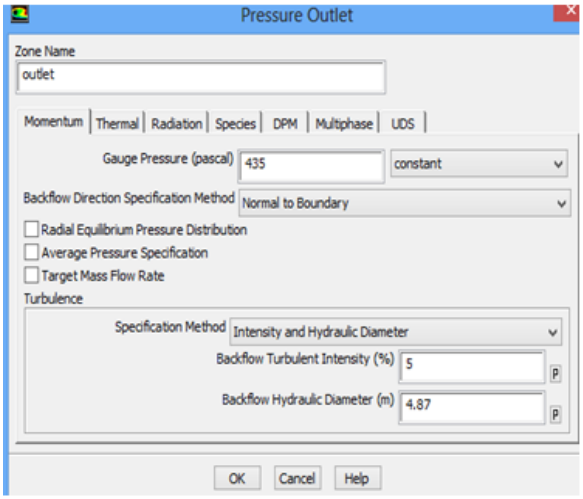

Outlet Boundary Condition

Figure 5.6 Boundary conditions for the base case

5.4 Postprocessing of Results for Base Case

Before discussing these results, it is important to mention here that first, the base case is simulated, and then a set of parametric studies are performed. In each case, a single parameter of the model is changed, then the model is executed, the results of these changes are compared with those of the base case, and the process is repeated for different parameters/components of the blower fan model. These different simulation results are discussed in the following subsections.

5.4.1 Velocity Contours

The velocity contours are given in Figure 5.7. The velocity contours show that the velocity changes along the cross-section of the model. The velocity increases with a decrease in the cross-sectional area of the model and vice versa. The recirculation zone is visualized at the right angle turn near the outlet. The velocity magnitude is determined at different measuring stations of the base case (see Figure 5.8). Table 5.4 gives the velocity magnitude at all these stations.

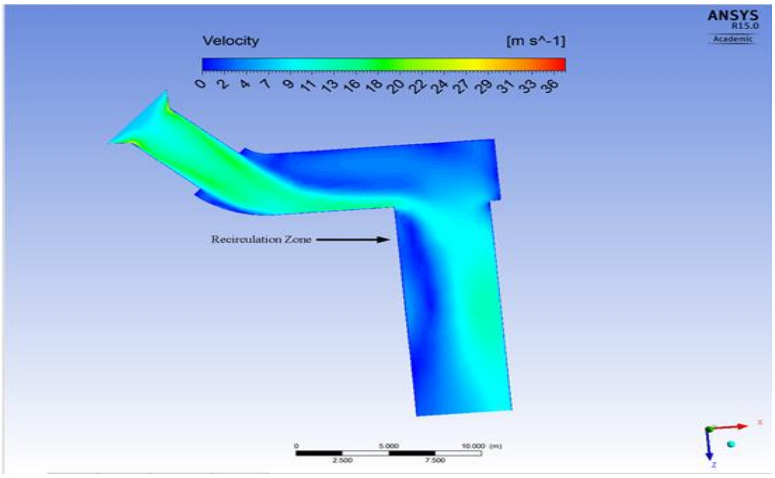

Figure 5.7 Velocity contours for the base case

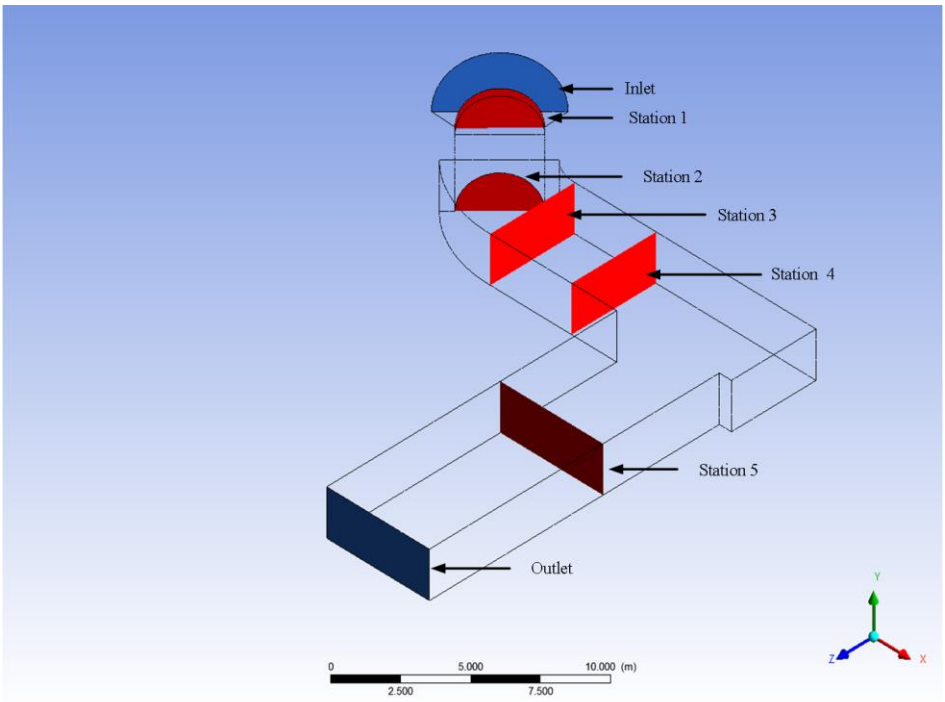

Figure 5.8 Measuring stations for the base case

Table 5.4 Velocity magnitude at different measuring stations

Stations	Velocity Magnitude (m/s)
Inlet	6.25
1	13
2	15
3	8
4	7.4
5	Turbulent
Outlet	5.56

5.4.2 Pressure Profiles

The pressure profiles for the base case are given in Figure 5.9 and their corresponding values are shown in Table 5.5. It is clear from the figure that the pressure decreases as the distance from the inlet increases. For example, at the distance of 7 m from the inlet, the static pressure is 469 Pa and pressure is dropped to 460 Pa at the distance of 9 m from the inlet.

Note that Table 5.5 gives the area average pressures at different locations of the model. It is impossible to measure the pressures at the straight and elbow duct of the base case. The main reason is due to the recirculation of the air. This problem is often avoided by increasing the distance between the outlet and the recirculation zone by three or four times the hydraulic diameter of the outlet boundary.

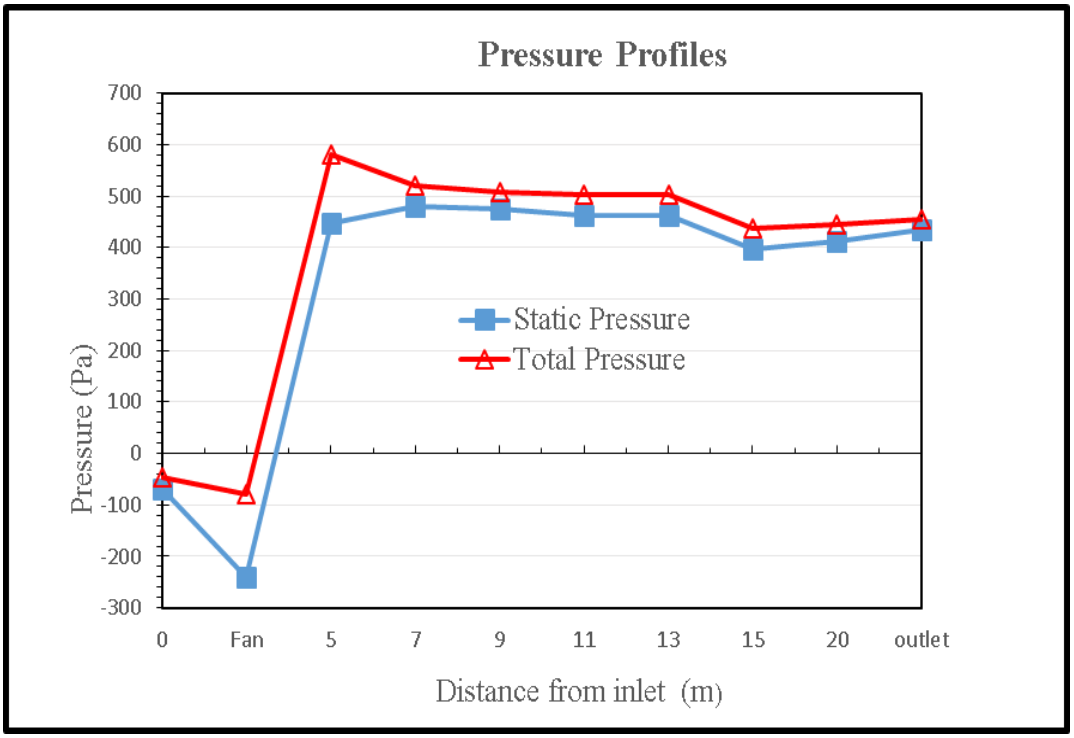

Figure 5.9 Pressure profiles for the base case

Table 5.5 Static and total pressure values

Distance from inlet (m)	Static Pressure (Pa)	Total Pressure (Pa)
Inlet	-70	-46
Fan	-237	-77
5	448	580
7	469	525
9	460	507
11	Turbulence	Turbulence
13	Turbulence	Turbulence
15	Turbulence	Turbulence
20	Turbulence	Turbulence
25	435	454

5.4.3 Flowrate Measurements

In this simulation, the flowrates were calculated at different sections of the mine. Flowrate at the inlet and outlet were 113 m^3/s and 123 m^3/s, respectively. This difference is due to recirculation of air near the outlet boundary of the base case.

A detailed calculation of the flowrates is given in Table 5.6. The velocity near the outlet of the base case is not determined due to the recirculation of the air. Therefore, the airflow near the outlet of the base is not determined.

Table 5.6 Pressure and air quantity values at different locations

Distance from inlet (m)	Static Pressure (Pa)	Total Pressure (Pa)	Area (m^2)	Air Quantity (m^3/s)
0	-70	-46	18	113
Fan	-241	-79	7.06	115
5	448	580	7.06	104
7	481	520	16	127
9	474	508	16	119
11	Turbulent	Turbulent	16	-
13	Turbulent	Turbulent	16	-
15	Turbulent	Turbulent	22	-
20	Turbulent	Turbulent	22	-
25	435	454	22	123

5.5 Parametric Studies

Four different parameters were analyzed and studied. The results of each of these parameters are compared with the base case. They are further discussed in the subsection 5.6. For each parametric analysis, only one of the parameters was changed at a time.

None of the simulation results were mesh independent because the mesh independent simulation results require a large amount of computational memory. In order to deal with this problem, only relatively parametric analyses were performed. Similarly,

in order to determine the air quantity for the given fan pressure, the intake fan pressure boundary was used. This gives the quantity of air for the given fan pressure. In this way, any improvement made in the model should increase the quantity of airflow.

5.5.1 Case 1: Increasing the Length of the Fan's Diffuser

In the first parametric analysis, the length of the diffuser was increased to 10 m. Figure 5.10 shows the geometry of case 1. The other dimensions of the fan components do not change and remain the same (for detail refer to Table 5.2).

The pressure values at different sections are given in Table 5.7. These are the average pressure values and are measured at different locations of the inlet. The pressure profiles for case 1 is given in Figure 5.11.

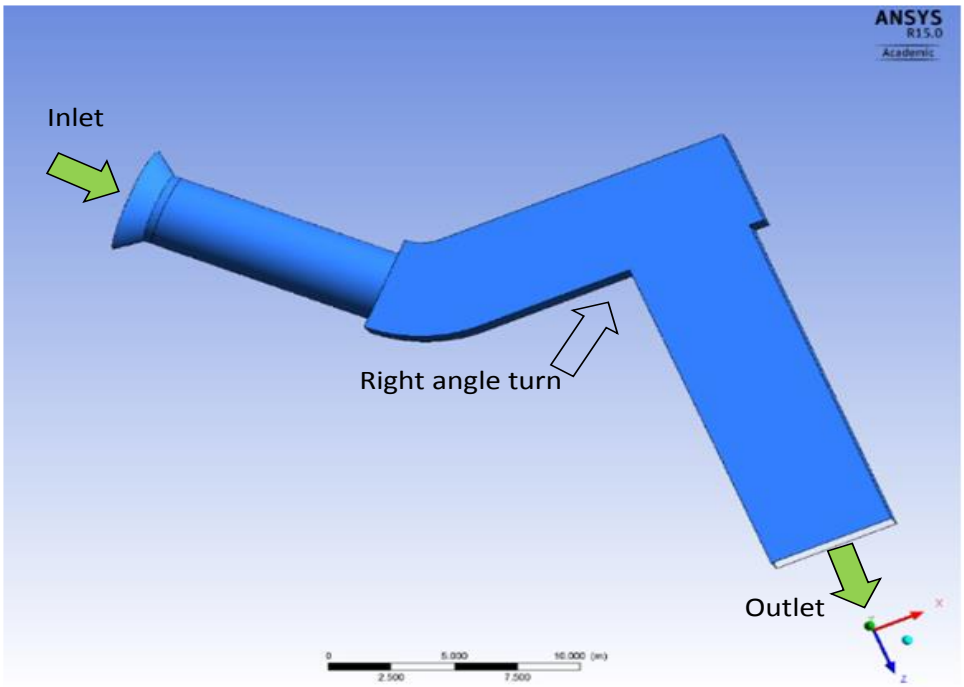

Figure 5.10 Geometry for the case 1

Table 5.7 Static and total pressure values for case 1

Distance from inlet (m)	Static Pressure (Pa)	Total Pressure (Pa)
0	78	118
Fan	-162	78
5	467	677
10	451	587
11	483	558
15	487	556
20	490	556
27	Turbulent	Turbulent
30	437	464

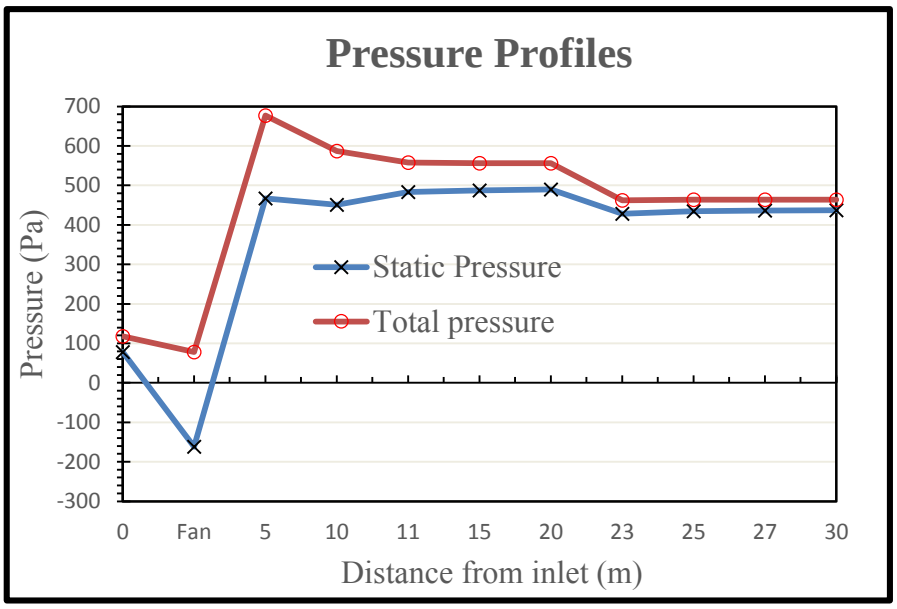

Figure 5.11 Pressure profiles for the case 1

The velocity contours for this case (see Figure 5.12) show there is a small recirculation of air near the outlet boundary zone when compared to the base case. The possible reason for a smooth and stable flow characteristic is that the increase in the length of the fan diffuser stabilizes the air. This is also evident by the study of the pressure profiles (see Figure 5.11).

The increase in the static pressure and decrease in the velocity pressure (details of the velocity magnitude and calculation for the flowrate are given in Table 5.8.) near the outlet zone also suggest that less eddies are developed near the outlet zone. However, a finer mesh is required to study the flow behavior near the outlet zone.

Another important fact that affects the flow characteristics at the outlet zone is the turbulence model selected for the simulation. A discussion on the different turbulence models and their merits are beyond the scope of this work.

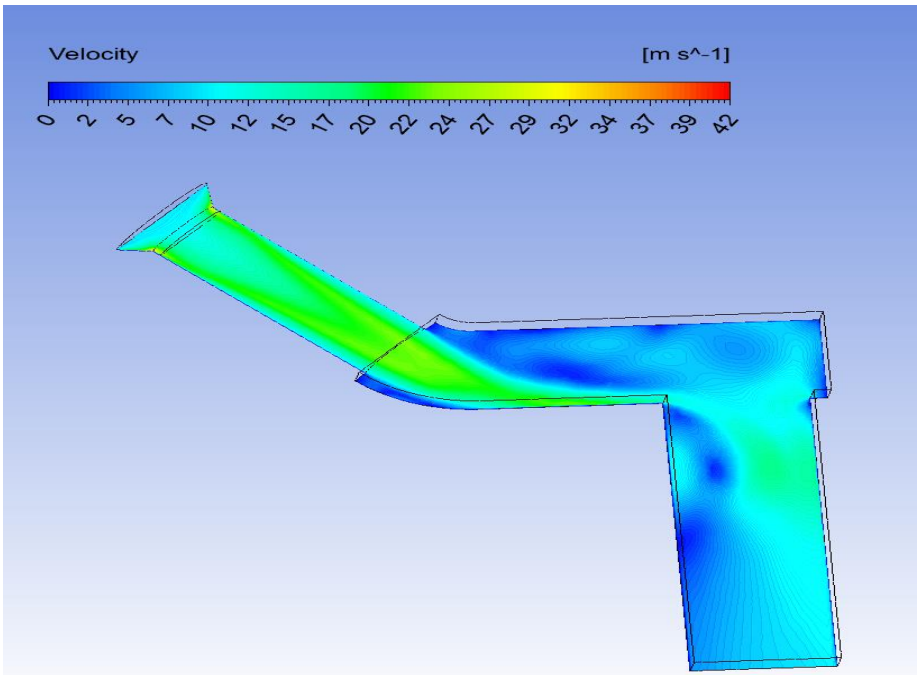

Figure 5.12 Velocity contours for the case 1

Table 5.8 Velocity and air quantity calculations

Distance from inlet (m)	**Velocity (m/s)**	**Area (m^2)**	**Air Quantity (m^3/s)**
0	8.1	18	145
Fan	19.79	7.06	140
5	18.52	7.06	131
10	15	7.06	105
30	6.64	22	146

5.5.2 Case 2: Changing the Straight Duct into a Curved Duct

In the second parametric study, the right angle turn (close to the outlet end) is avoided by a curving elbow duct located near the outlet. Figure 5.13 shows the geometric model for this parametric case.

The simulation was done under the same conditions used in the base case. As a result of the change in the geometry, the air quantity increased by 13 % when compared with the base case. Static and total pressure values at different sections of the model are given in Figure 5.14. Also note that pressure losses are mainly due to a change in the airflow direction.

As mentioned in the above paragraph, refer to Figure 5.14 for pressure profiles. Figure 5.15 shows the velocity contours for case 2. The air tends to recirculate at the straight duct section of the installation (see Figure 5.15). However, this recirculation of the air is small when compared to the base case. Table 5.10 gives average area weighted velocities and the air flowrate quantity at different sections for this model.

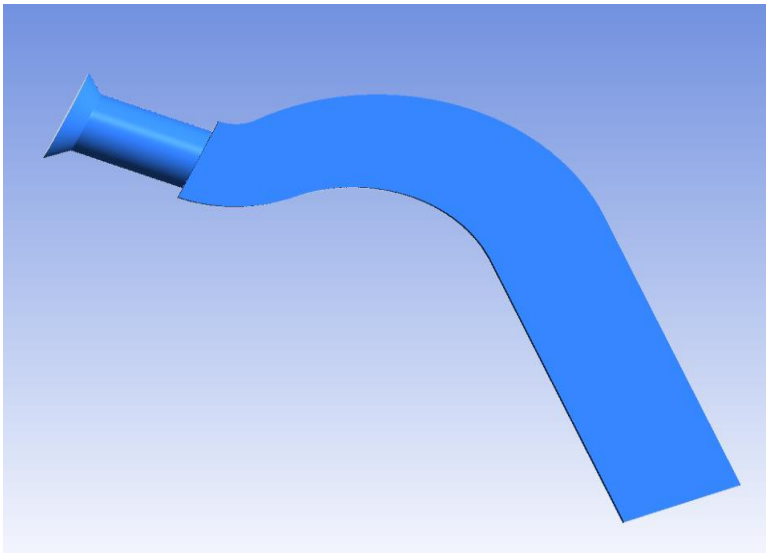

Figure 5.13 Geometry for the case 2

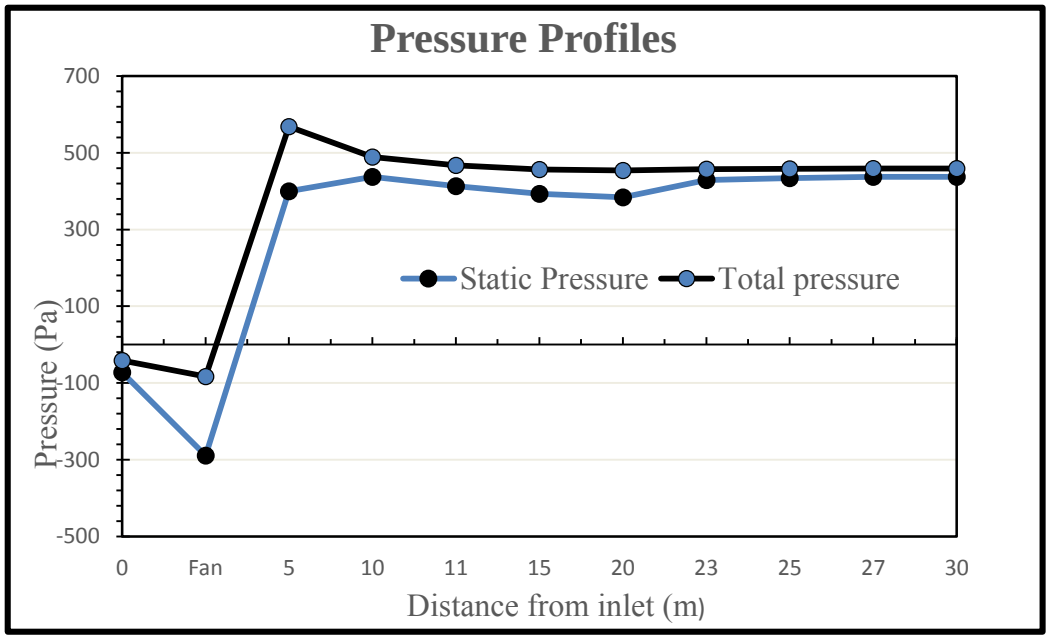

Figure 5.14 Pressure profiles for the case 2

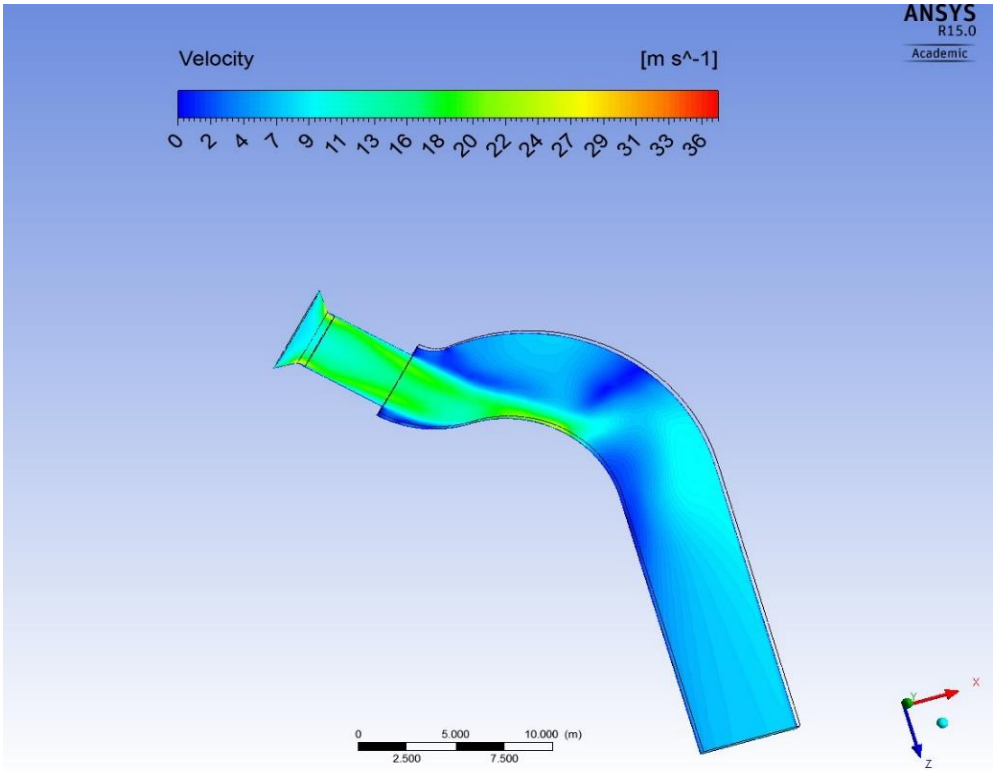

Figure 5.15 Velocity contours for the case 2

Table 5.9 Velocity and flowrate calculations

Distance from inlet (m)	**Velocity (m/s)**	**Area (m^2)**	**Air Quantity (m^3/s)**
0	7	18	126
Fan	18	7.06	127
5	17	7.06	120
7	9	16	144
9	9	16	144
11	Turbulent	22	-
13	Turbulent	22	-
15	Turbulent	22	-
20	6	22	132
25	6	22	132
30	6	22	132

5.5.3 Case 3: Changing the 90 Angle Turn to 135°

For the third case, the right angle turn for the base case has been changed to 130°. This change in the angle is shown in Figure 5.16. As a result of this change in geometry, velocity at the inlet increased to 6.4 m/s. The calculated air quantity is 114 m^3/s. This means an increase of 4 m^3/s of air quantity when compared with the base case. It should be noted that the fan pressure will hold constant in all the cases with only the degree angle as the variable.

The velocity contours for this case are given in Figure 5.17 and for the pressure profiles, refer to Figure 5.18. The velocity contours show that most of the air tends to slip away from the 130 ° corner toward the exterior corner. A finer mesh size is required to study the air behavior at the 130 degree corner. The details of the pressure, velocity, and the air flowrate are given in Table 5.10.

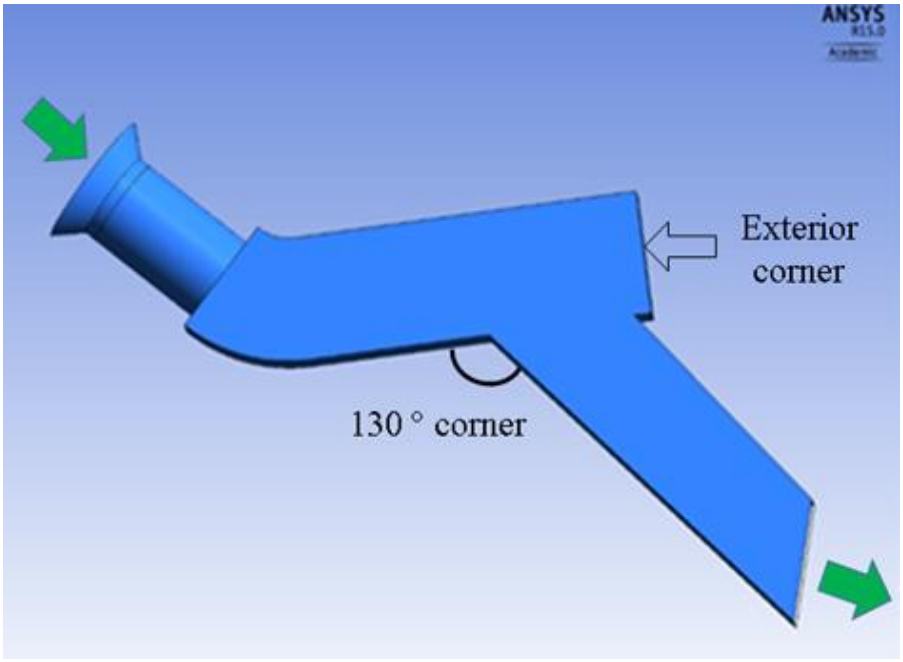

Figure 5.16 Geometry for the case 3

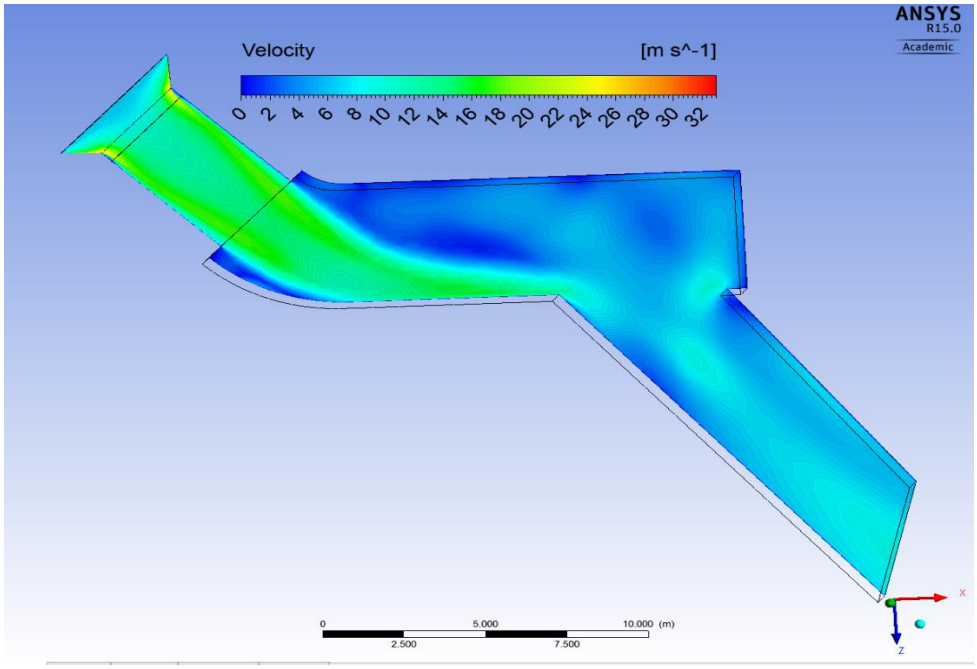

Figure 5.17 Velocity contours for the case 3

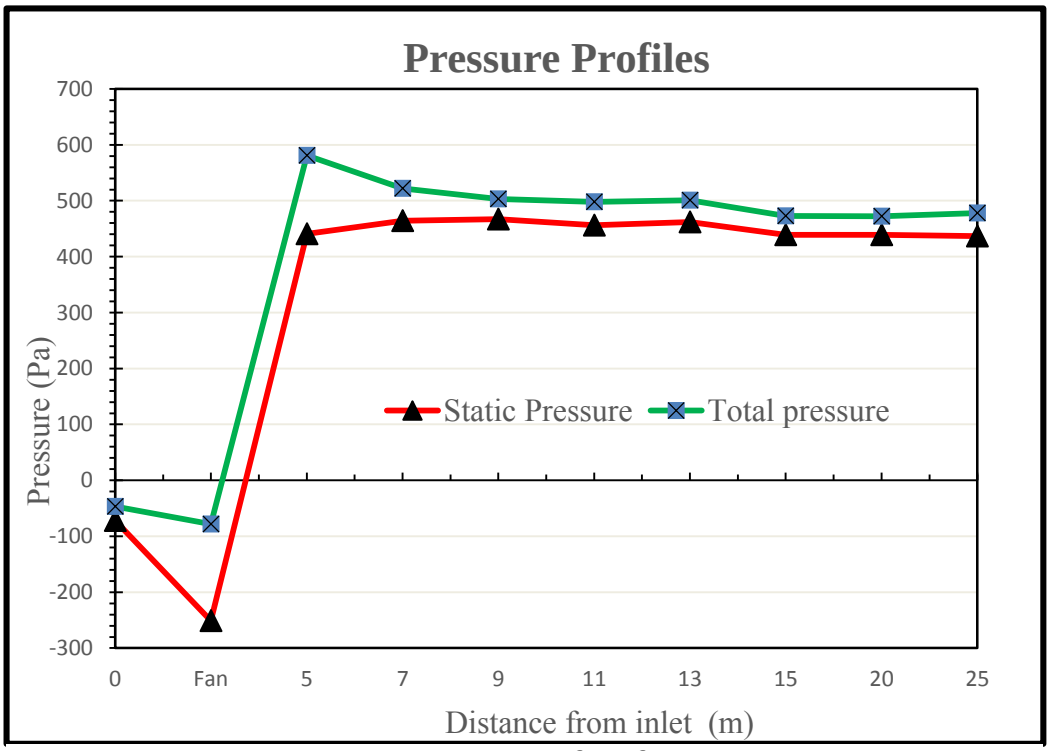

Figure 5.18 Pressure profiles for the case 3

Table 5.10 Pressure, velocity, and flowrate calculations

Distance from inlet (m)	**Static Pressure (Pa)**	**Total Pressure (Pa)**	**Velocity (m/s)**	**Area (m^2)**	**Air Quantity (m^3/s)**
0	-72	-47	6.39	18	115
Fan	-251	-78	16.81	7	118
5	441	581	15.12	7	107
7	464	522	9.73	16	155
9	467	503	7.67	16	123
11	456	498	8.28	16	132
13	462	501	7.98	16	128
25	Turbulent	Turbulent	-	22	-

5.5.4 Case 4: Increasing the Outlet Length

In this case, the length of the outlet is increased by two times the hydraulic diameter of the outlet. The geometry of this case is given in Figure 5.19. A velocity of 6.2 m/s was calculated using the fan intake pressure. This gives a reading of 112 m^3/s, the same quantity of the air that was measured in the base case. Also, with an increase in the outlet cone, the size of the recirculation zone in case 4 has also increased (see Figure 5.20 for velocity contours).

It means that for both the base case and case 4, the air flow near the outlet zone is not fully developed. Any measurement made in the recirculation zone is prone to errors. For the pressure profile, refer to Figure 5.21. The pressure, velocity, and air quantity at different locations for case 4 is given in Table 5.11.

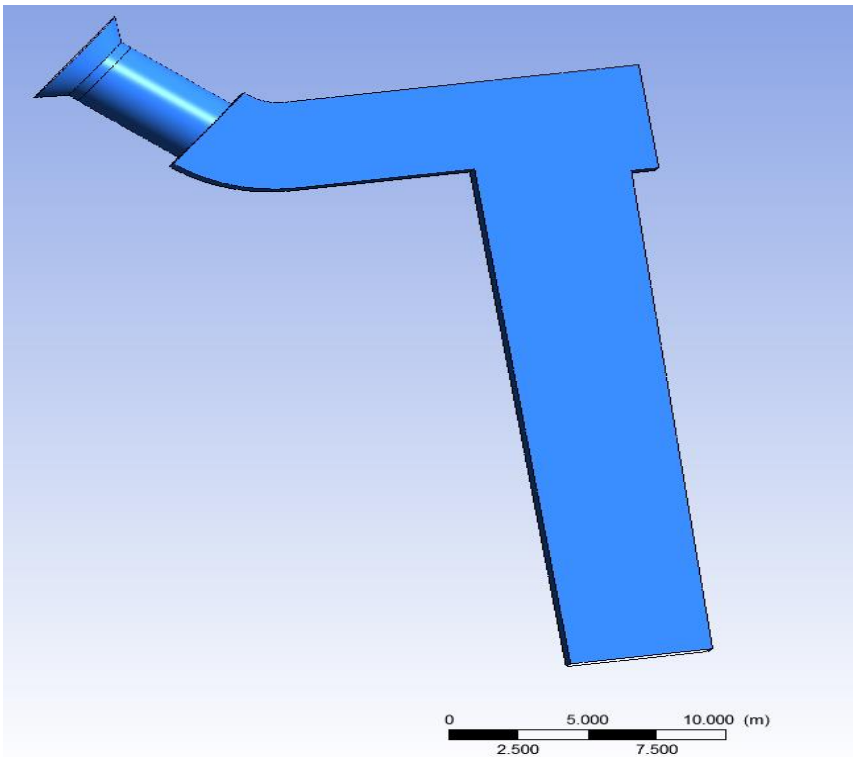

Figure 5.19 Geometry for the case 4

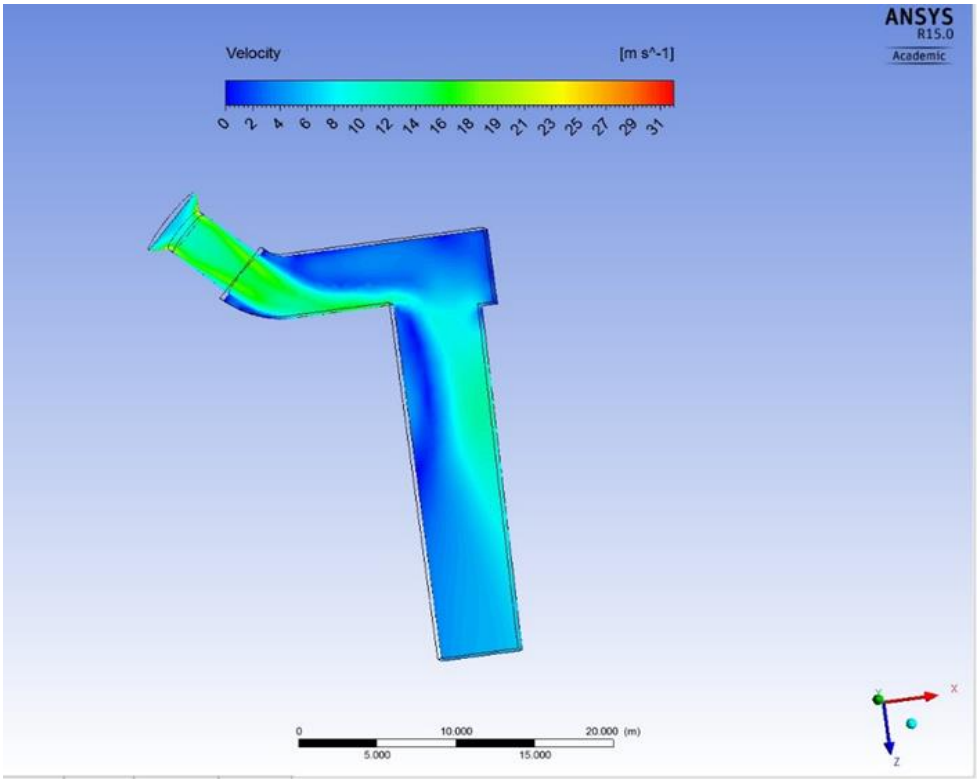

Figure 5.21 Velocity contours for the case 4

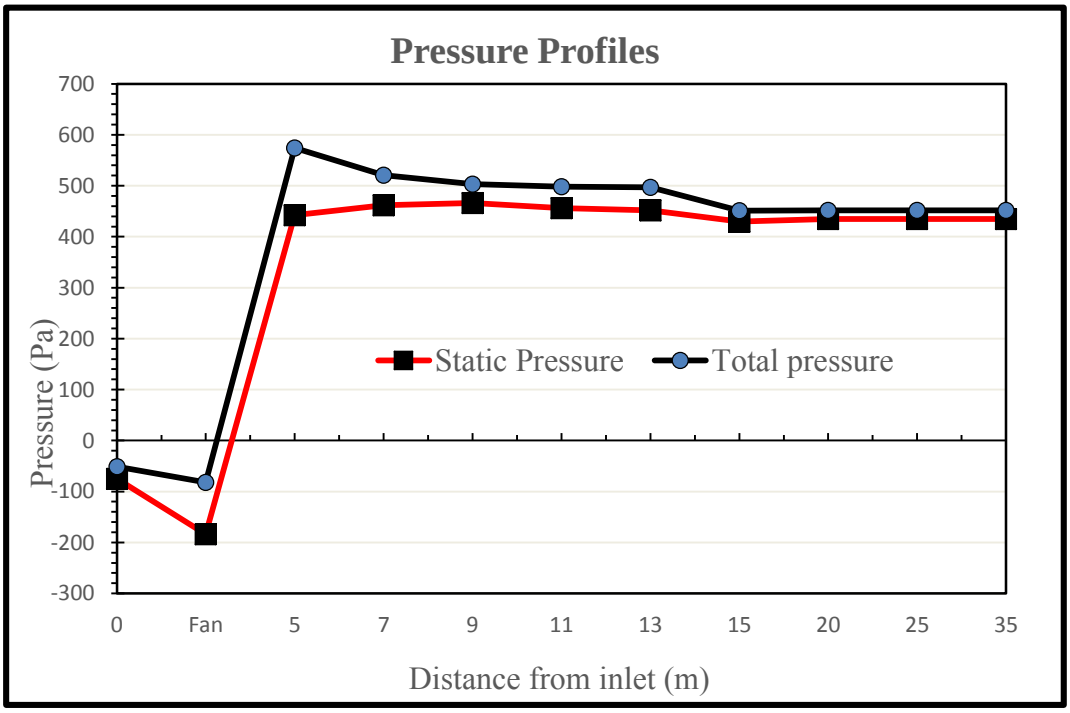

Figure 5.20 Pressure profiles for the case 4

Table 5.11 Pressure, velocity, and air quantity for case 4

Distance from inlet (m)	Static Pressure (Pa)	Total Pressure (Pa)	Velocity (m/s)	Area (m^2)	Air Quantity (m^3/s)
0	-75	-51	6.25	18.678	117
Fan	-184	-82	12.90	8.064	104
5	442	574	14.68	8.044	118
7	462	521	9.81	17.976	176
9	466	503	7.77	17.61	137
11	Turbulent	Turbulent	8.28	17.61	-
25	Turbulent	Turbulent	5.26	22.34	-
30	435	452	5.26	22.074	116

5.6 Conclusion

The base model shows a pressure loss due to the geometry of the fan installation. A significant source of pressure loss is at the right angle turn at the recirculation zone. As explained above, any measure made to the recirculation zone is not free from errors. This is due to instability in the air flow caused by recirculation of air. The main purpose of this research study is to make improvements to the fan installation. Any improvements made in the blower model should increase the air quantity. This parametric analysis shows that the air quantity is increased in all cases except in case 4. However, case 1 had the highest flowrates. This case also had a smaller recirculation zone when compared with the base case. A final recommendation of this blower system installation is to increase the fan's diffuser length and change the right angle turn to an obtuse angle. This will ensure a smooth flow of air inside the fan installation.

Furthermore separate parametric studies can be done to determine the optimum obtuse angle that can replace the right angle turn. The optimum obtuse angle for this case will significantly increase the airflow quantity, as the right angle turn is one of the major sources of the shock loss. The study has also found that the right angle turn tends to produce more shock losses than the obtuse angle; therefore, increase the fan distance for the right angel turn and then change the right angle turn to optimum obtuse angle.

CHAPTER 6

MINE B: EXHAUST SYSTEM

In Chapter 5, a blower system installation was discussed. In that particular fan installation, it was found that increasing the length of the fan outlet duct (diffuser) and changing the outlet angle increased the airflow quantity into the mine. In this chapter, parametric analyses will be performed for an exhaust fan system. The main difference between a blower system and an exhaust system is that in an exhaust system, the fan develops a negative pressure and pulls the air out of the mine into the atmosphere.

The geometry of the fan installation for this system consists of a mine shaft, fan house, fan duct, and an evasée. When this system is not installed adequately, a significant portion of the fan pressure is lost at the fan house. As in Chapter 5, the problem is investigated using CFD. For a sample mine, first, the geometry of an exhaust system was generated, next, the boundary conditions defined, and finally, the CFD model was simulated using FLUENT.

Analyzing the results of the model showed that the fan performance was subjected to shock losses due to obstructions in the air path near the fan installation. These shock losses can be reduced by correct fan ductwork arrangement, and proper evasée design (for more details of fan ductwork, refer to Chapter 2).

6.1 Geometry of the Exhaust System

The geometry of the exhaust system installation consists of a ventilation shaft, a fan house, a weak wall, fan inlet and outlet ducts, a fan, and a vertical evasée. For this exhaust system installation, the shaft is 5 m in diameter and 15 m in length. It has a fan house at the top of the shaft. The fan house protects the shaft, shaft collar, and the turning vanes. The fan house is also equipped with an access airlock door system, and a weak wall.

The main purpose of the doors is to provide access to the maintenance crew. It also protects from intrusion by any unwanted person or object. At the top of the fan house is the weak wall. The purpose of the weak wall, as explained in Chapter 2, is to protect the fan installation and the fan itself from explosive waves. However, in this study, the weak wall is not simulated since the simulation of the weak wall requires a solver to solve the governing equation for the porous medium. The study of the porous media is beyond the scope of this research.

The fan house is connected to the fan though an inlet duct. For the base case, there is no ductwork (refer to Chapter 2) between the fan house and fan. It means that the fan is connected to the fan house though an inlet cone. The outlet of the fan is connected to a vertical evasée. Finally, the fan installation ends with the outlet of a vertical evasée.

The geometry of each component was created using ANSYS's Design Modeler (see Figure 6.1). For the dimensions of the model, refer to the Table 6.1. The dimensions of the fan installation are chosen to mimic an actual fan installation observed in a U.S. coal mine. For parametric analysis, the dimensions of fan installation components are not changed except for the component under investigation.

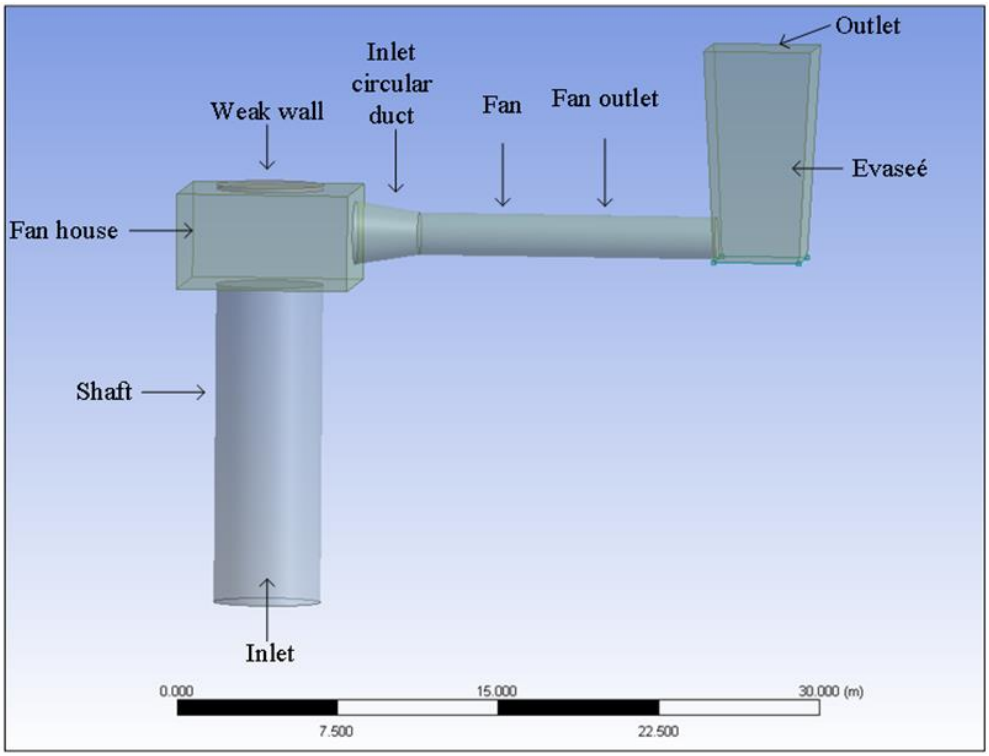

Figure 6.1 Geometry of the exhaust system

Table 6.1 Dimensions for different components

Parts/ Components	**Dimensions/ Descriptions**
Shaft	diameter= 5m and length = 15 m
Fan house	Length = 4 m , width = 4m and height = 4 m
Weak wall	Porous media, not simulated
Inlet circular duct	Length = 3 m
Fan	diameter = 2 m, fan pressure = 700 Pa
Fan outlet duct	Length = 10 m and diameter = 2 m
Evasée	Length = 15 m

Mesh grids, defined in Chapter 5, are important for solving the governing equation behavior at different sections of the base case installation. Therefore, it is important to generate good quality mesh to get accurate result. The mesh quality is also important for convergence of the solution as poor mesh quality tends to converge after a larger number of iterations or worse, the solution does not converge.

The mesh for the base case are shown in Figure 6.2. As is in Chapter 5, the geometry of the model is for a symmetric body. Therefore, Figure 6.2 shows the mesh grids on the symmetric axis. The default mesh generates unstructured mesh elements. They are tetrahedral in shape. The main disadvantage with the unstructured mesh is that it takes more time for a solver to converge the solution. For further details about the mesh quality boundary layers and mesh sizing, refer to Table 6.2.

In Table 6.2, the orthogonal quality indicates the quality of meshing. The orthogonal quality ranges between 0 and 1, where 0 orthogonal quality means the worst cell and a symmetric cell in the mesh has an orthogonal quality of 1. Further details about the mesh orthogonal quality is beyond the scope of this work.

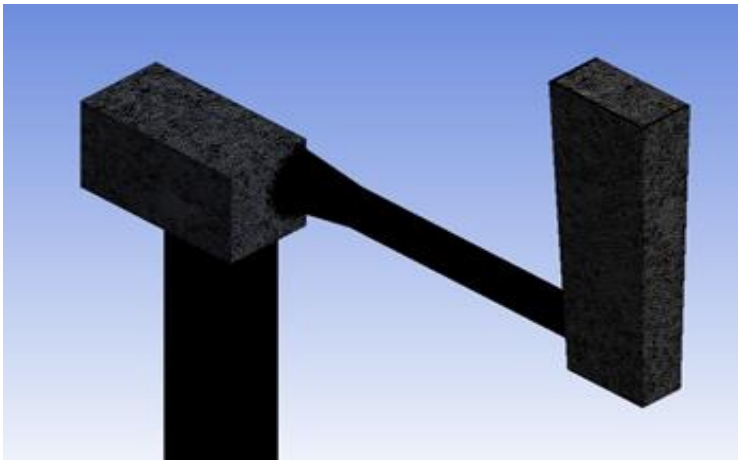

Figure 6.2 Surface mesh for the base case

Table 6.2 Summary of mesh setting

Components/Factors	Description
Maximum face size	150 mm
Mesh element growth rate	1.20
Number of boundary layers	5
Number of elements	8,088,412
Average cell orthogonal quality	0.894

6.2 Base Case Simulation

The simulation exercise presented in this chapter was performed using the same procedure described in Chapter 5. The main assumptions for this case are the same as those discussed in Chapter 4. The convergence of physical quantities also known as residuals indicates that the final results follow the law of physics (refer to Table 6.3 for the simulation parameters).

A standard k-epsilon turbulence model was used in all the simulation work in this chapter. The convergence criteria for this case is set to the third decimal place. Figure 6.3 shows that the residuals (velocity, mass, k, and epsilon) converge after 200 iterations.

For the first few iterations, there were reverse flows at the pressure outlet, causing a large residual fluctuation at the beginning of the process. However, the solution stabilizes with an increase in the number of iterations (refer to Figure 6.3 for details).

Table 6.3 Simulation parameters

Parameters	Values/ Descriptions
Turbulence model	Standard k- ε model
Wall treatment	Enhanced wall treatment
Material	air density = 1.225 kg/m^3, Viscosity = 2e-5 kg/m-s
Residuals convergence criteria	Velocities (x, y, and z) = 0.001 K and epsilon = 0.001 Mass = 0.001
Initialization method	From inlet

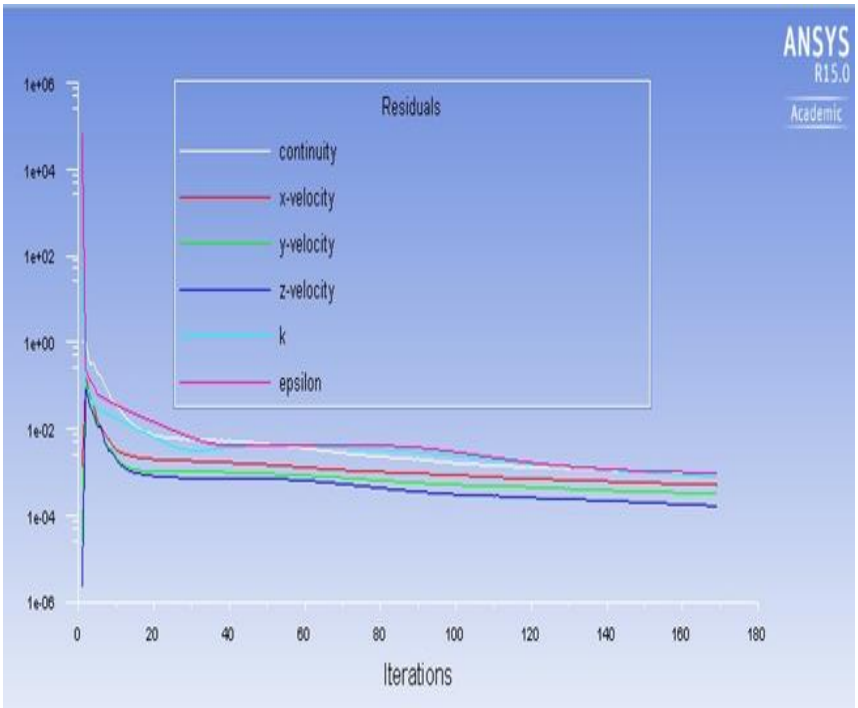

Figure 6.3 Residual plots for the base case

In a numerical simulation, the selection of correct boundary conditions is imperative to get an accurate solution. The boundary conditions as well as some other important parameters necessary for the simulation are discussed in the following subsections.

6.2.1 Boundary Conditions

As discussed in Section 6.2, boundary conditions are important parameters for any numerical simulation exercise. For an exhaust fan system, in a fashion similar to those discussed in Chapter 5, the parameters of interest include: inlet velocity, fan pressure, and outlet pressure. In order to determine the inlet velocity, two different simulation were performed with the same simulation parameters and fan pressure. For the first simulation, fan intake boundary at the inlet was examined (refer to Figure 6.4).

This simulation determined the velocity of the air for a given fan pressure. After determining the velocity at the inlet by using fan intake, a second simulation was performed under the same conditions. In the second simulation, velocity inlet, fan pressure, and pressure outlet were used as boundary conditions.

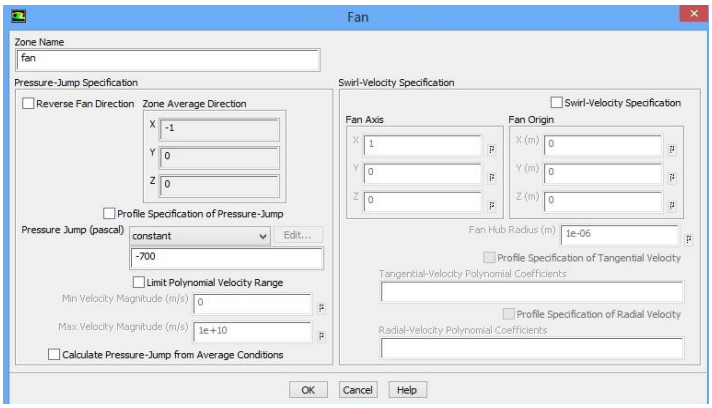

Figure 6.4 Fan intake boundary conditions

The simulation results for the base case are first analyzed in the following subsection, then these are compiled and plotted to be used as baseline figures when parametric studies are performed. The results presented in following subsections include: velocity contours, pressure profiles, and flow rates.

6.2.2 Velocity Contours and Streamlines

Figure 6.5 shows the velocity contours for the base case. The magnitude of this variable is stronger in the fan duct and at a minimum at the fan house and at the evasée. The velocity streamlines (see Figure 6.6) show the formation of large eddies and flow recirculation at the base of the evasée. The streamlines also show that the velocity magnitudes at the bottom of the evasée are higher than the velocity at the top of the evasée. As the air moves up towards the outlet, the air velocity decreases and the airflow quantity recirculates. The exact extent of the recirculation of air and its behavior at the evasée can be studied with a much finer mesh. However, finer mesh cannot be generated due to the limited computation memory of the hardware.

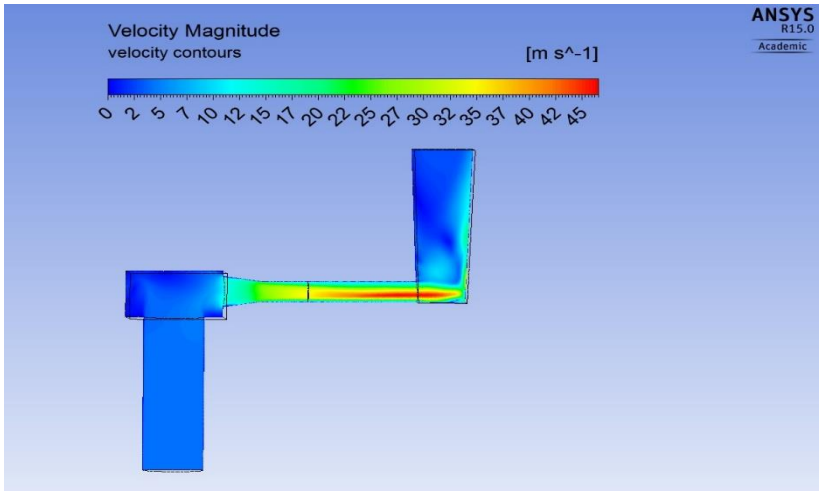

Figure 6.5 Velocity contours for the base case

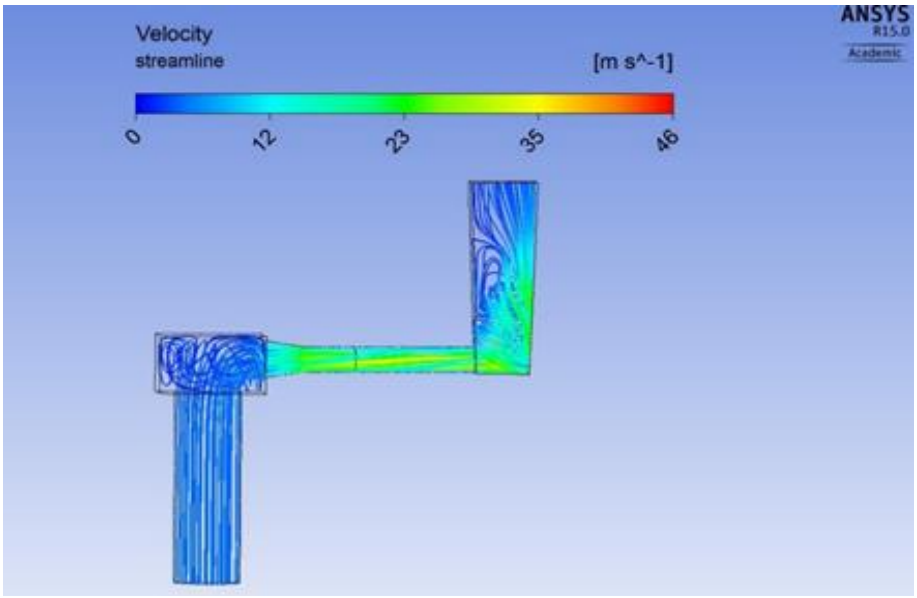

Figure 6.6 Velocity Streamlines for the base case

6.2.3 Pressure Profiles

The static and total pressures are measured by constructing polylines. The line starts from the inlet and ends at the outlet (see Figure 6.7). This line is 55 m in total length. Table 6.4 shows the reading at every 5 meters. Note that pressures measured at the evasée are prone to errors .The randomness in the air flow pattern makes it difficult to measure average pressures at the evasée. For this case, readings at the outlet of the evasée are taken into account. An evaluation of the pressure profiles (Figure 6.8), shows that there are also significant pressure losses in the fan outlet and at the evasée. However, the pressure loss at the evasée is less than the pressure loss at the fan house.

At the evasée, there is a pressure loss of 423 Pa in the fan evasée (refer to Figure 6.8). This loss of pressure is mainly due to the shock loss at the evasée. Average values of the total and static pressure are given in the Table 6.4.

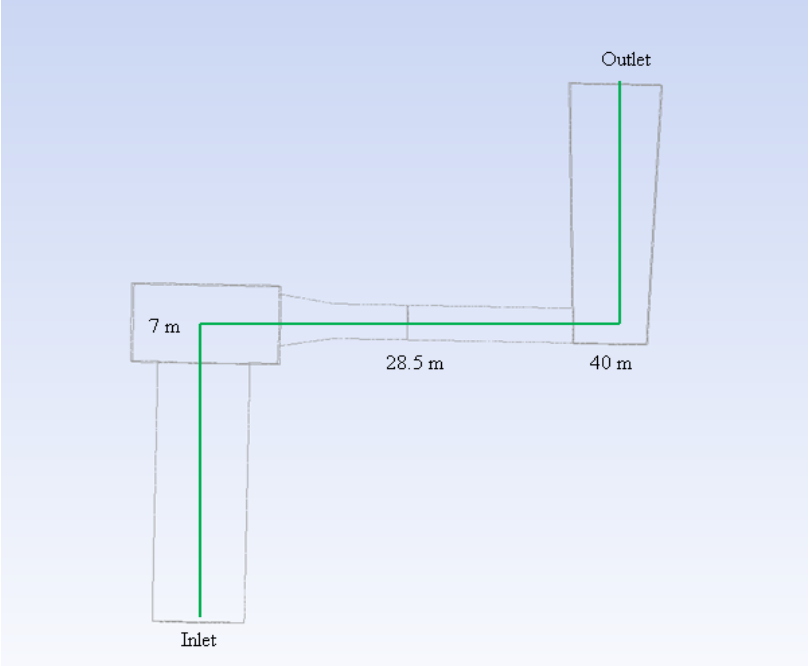

Figure 6.7 Construction of the line for measuring pressure

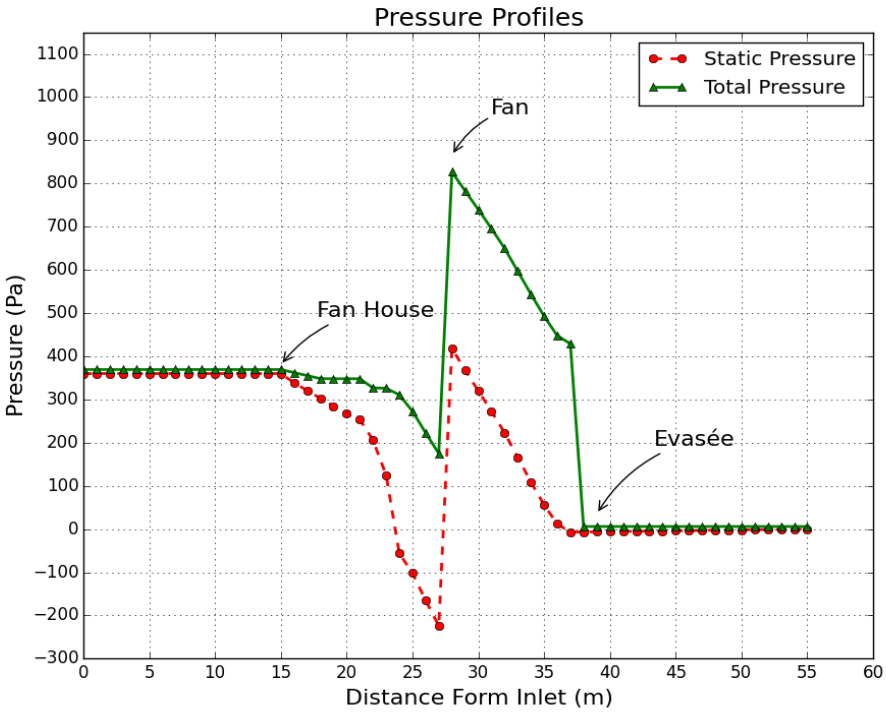

Figure 6.8 Pressure profiles for the base case

Table 6.4 Static and total pressure values

Distance from Inlet (m)	Static Pressure (Pa)	Total Pressure (Pa)
0	360	369
5	360	369
10	360	369
15	360	369
20	264	349
25	-103	271
30	320	737
35	58	490
40	Turbulent	Turbulent
45	Turbulent	Turbulent
50	Turbulent	Turbulent
55	0	3.16

6.2.4 Flowrate

The flowrates at different sections of the base case installation were determined by slicing a plane at different sections of the installation (see Figure 6.9). Refer to Table 6.5 for the cross-sectional area, pressure values, and the flow rates. For each section, the flow rate was determined by multiplying the average air velocity by the cross-sectional area at that station. The flowrate at the inlet was 77 m^3/s and flowrate at the outlet is about 79 m^3/s. This difference between the inlet and outlet is due to recirculation. Note that in Figure 6.9, the model has been sliced by the centerline in order to save the computational memory while performing the numerical simulations. However, the calculations in Table 6.5 are for the full model.

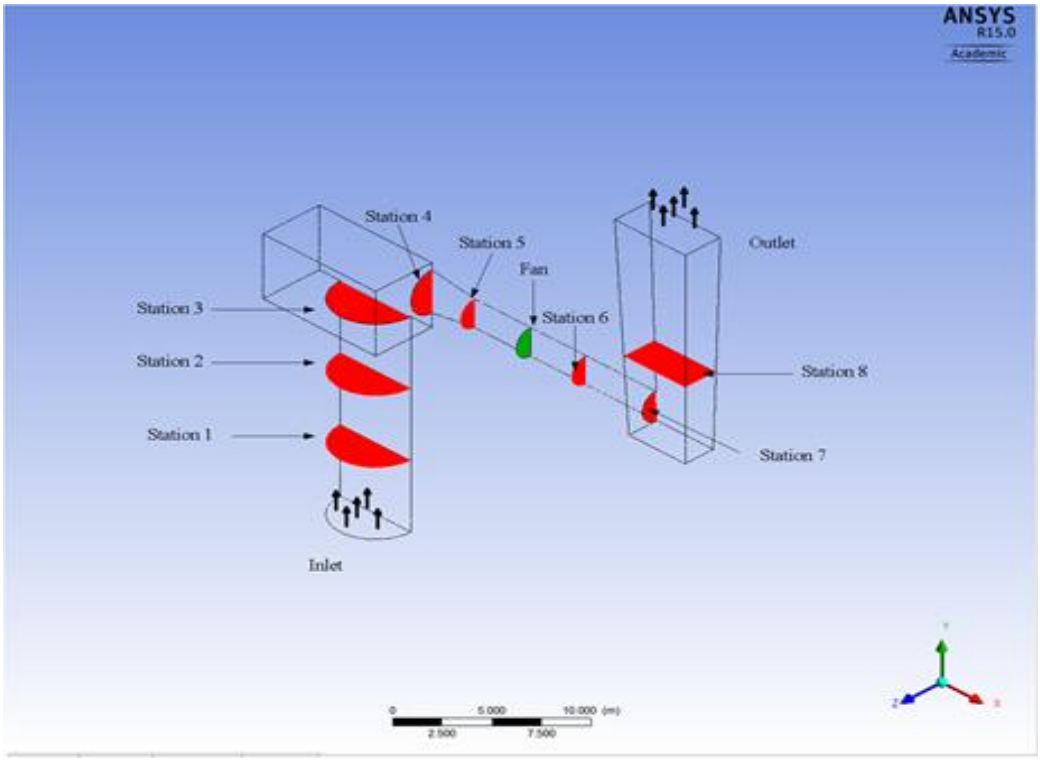

Figure 6.9 Measuring station for the base case

Table 6.5 Pressure and flowrate measurements

Measuring Stations	Static Pressure (Pa)	Total Pressure (Pa)	Velocity (m/s)	Area (m^2)	Flowrate (m^3/s)
Inlet	360	369	3.9	19.63	77
1	360	369	3.9	19.63	77
2	360	369	3.9	19.63	77
3	360	369	3.9	19.63	77
4	289	360	11	7.04	76
5	-103	271	25	3.14	78.7
6	221	653	26	3.14	83
7	Turbulent	Turbulent	Turbulent	3.14	Turbulent
8	Turbulent	Turbulent	Turbulent	19	Turbulent
Outlet	0	6.13	3.16	25	79.05

6.3 Parametric Studies

Parametric studies were conducted to improve the fan installation, thus improving the fan performance. Two cases are considered. In the first case, to reduce shock losses, the fan outlet duct and the evasée were connected through a gradual expansion cone. All other installation components remained unchanged. In case 2, the rectangular evasée is replaced by rounded conical evasée. Beside the changes in the evasée, changes in the fan ductwork, discussed in Chapter 2, were included in the simulation models.

6.3.1 Case 1: Installation of an Expansion Cone

In this case, an expansion cone is inserted between the fan outlet duct and the evasée (see Figure 6.10). The purpose of this change is to recover part of the shock loss that takes place between the fan outlet and the evasée. Other parameters such as mesh size, fan pressure, and air properties were not changed. This consistency is maintained to ensure that the results of this case can be compared with those of the base case.

As mentioned earlier, Figure 6.10 shows the geometry for case 1. Note that for this case, the length of the evasée is increased to counter the air reversal at the evasée outlet. The dimensions of case 1 is given Table 6.6. Shaft diameter and the length remains unchanged in all the parametric analyses.

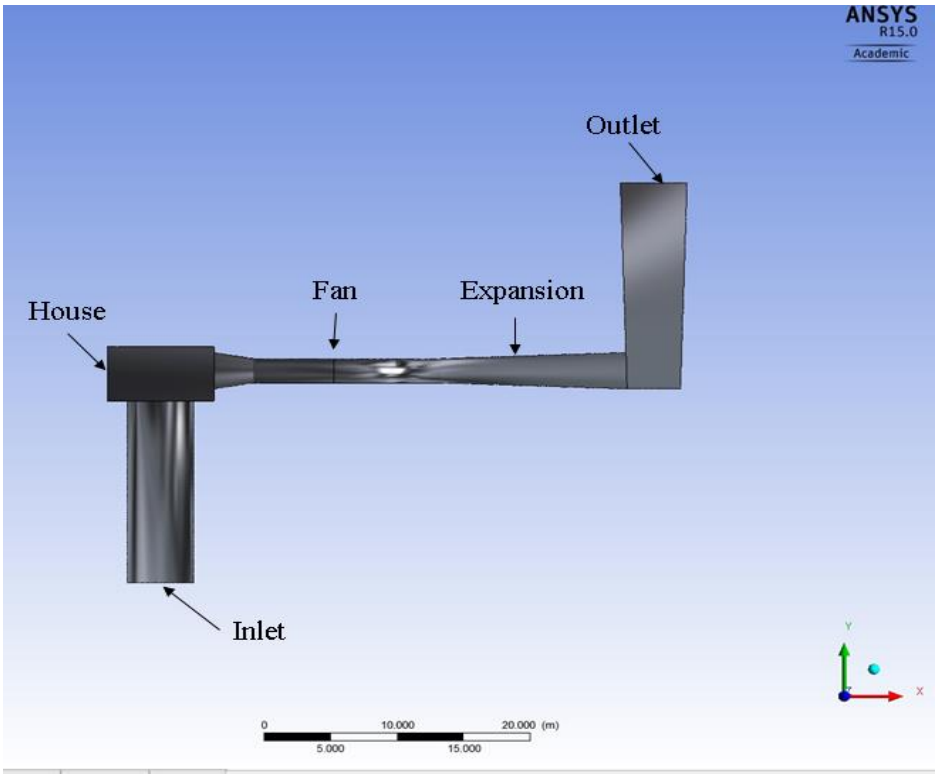

Figure 6.10 Geometry for the case 1

Table 6.6 Dimensions for different components

Components	Dimensions
Shaft	Diameter = 5m, Length = 15 m
Fan house	Length x Height x Width = 4 x 4 x 4 m^3
Expansion cone	Length = 14 m, inlet cone diameter = 2 m, and outer cone diameter = 3 m
Evasée	Length = 15 m

6.3.1.1 Velocity Contours and Streamlines for Case 1

Velocity contours whose contours define the velocity magnitude at different sections of the flow. Figure 6.11 shows the velocity contours for this case 1. Similar to the base case, the velocity is stronger at the fan outlet duct and weaker at the evasée and fan house. At the shaft, the velocity remains constant. The average velocity at the shaft is 3 m/s. The velocity streamlines are shown in Figure 6.12. The streamlines show air reversal at the outlet.

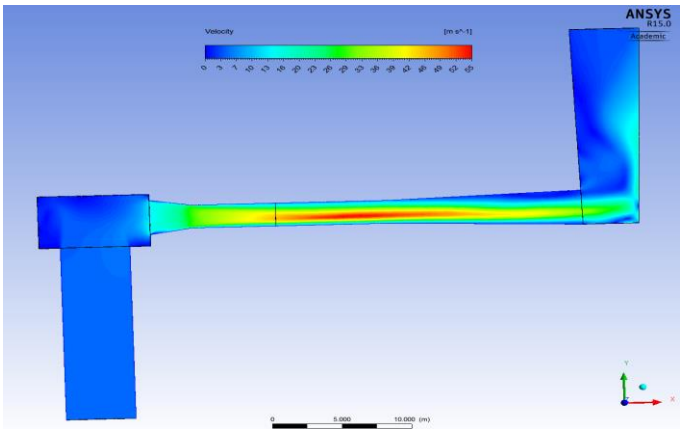

Figure 6.11 Velocity contours for the case 1

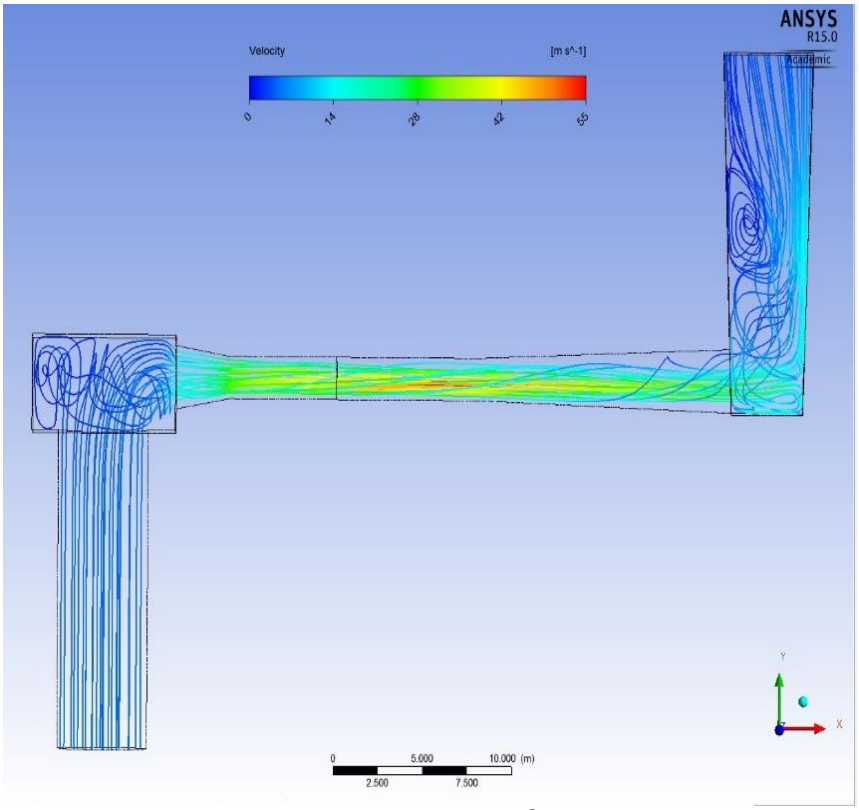

Figure 6.12 Velocity streamlines for the case 1

6.3.1.2 Pressure Profiles for Case 1

Figure 6.13 shows the static and total pressure profiles for this case 1. Based on these profiles, it can be concluded that most of the pressure losses take place at the fan evasée. A large percentage of these losses are mainly caused by shock losses. At the expansion zone, part of the static pressure is recovered. This recovery in the pressure is evident by the increase in the static pressure. There is also a small pressure loss in the evasée as compared to the base case.

This is due to the expansion cone inserted between the fan outlet and the evasée. When compared to case base, the installation of the expansion cone reduces the shock losses at the evasée is 120 Pa (refer to Figure 6.8 for the pressure profiles of the base case).

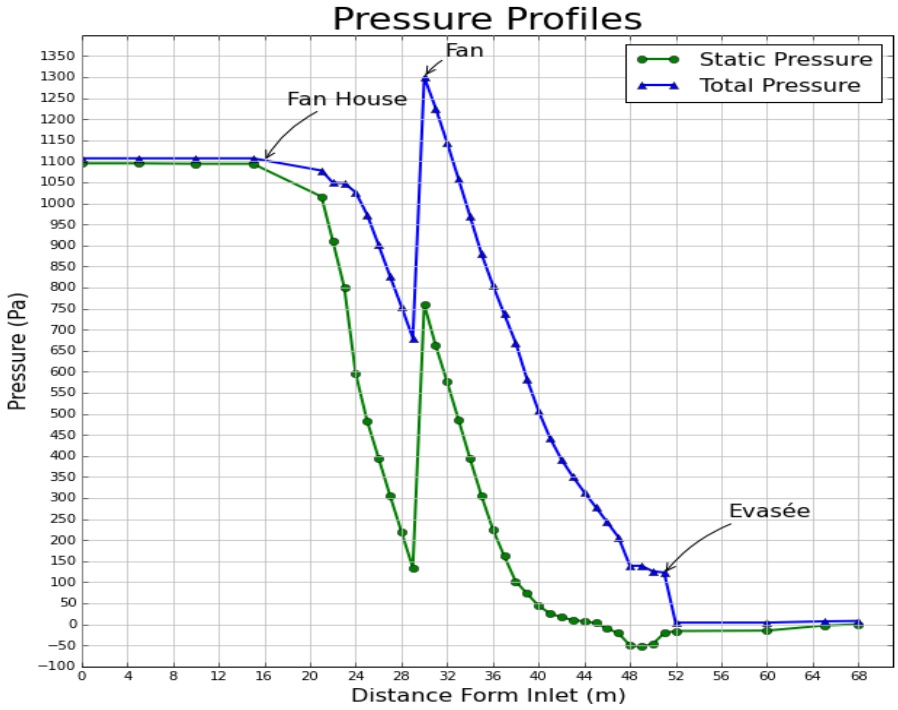

Figure 6.13 Pressure profiles for the case 1

6.3.1.3 Flowrate Calculation for Case 1

The values of the velocities, and flowrates at different sections in the installation are given in Figure 6.14. The flowrate in case 1 measured at the inlet and outlet is 88 m^3/s. The flowrate for the base case in 77 m^3/s. This means that there is about 13 % increase in the flowrate for the expansion cone.

6.3.2 Case 2: Installation of Expansion Cone and Fan Ductwork

For this case, the rectangular evasée was replaced with a conical one. The change in geometry of the evasée is made in order to study the effect of the shape of evasée on pressure losses. Another change to the model was the insertion of a ductwork between the fan outlet and the evasée. Figure 6.15 shows the modified geometry of the model. Furthermore, the fan outlet duct is connected to the conical evasée through an expansion cone. The length of the transition piece from rectangular to circle ductwork is 4 m and the length of expansion cone is 14 m.

The diameter of circular evasée is 5 m and the length of the circular evasée is about 8 m (see Table 6.7 for other dimensions). In this case, the evasée is not horizontal but rather tilted at an angle of 45° from the horizontal plane. The geometry of the upstream section, including the shaft and fan house, remained unchanged.

Table of Design Points

	A	B	C	D	E
1	Name	P35 - flowrate at inlet	P36 - flowrate at outlet	Exported	Note
2	Units	m^3 s^-1	m^3 s^-1		
3	Current	44.176	-44.174		
*				☐	

Figure 6.14 Flowrate for the case 1

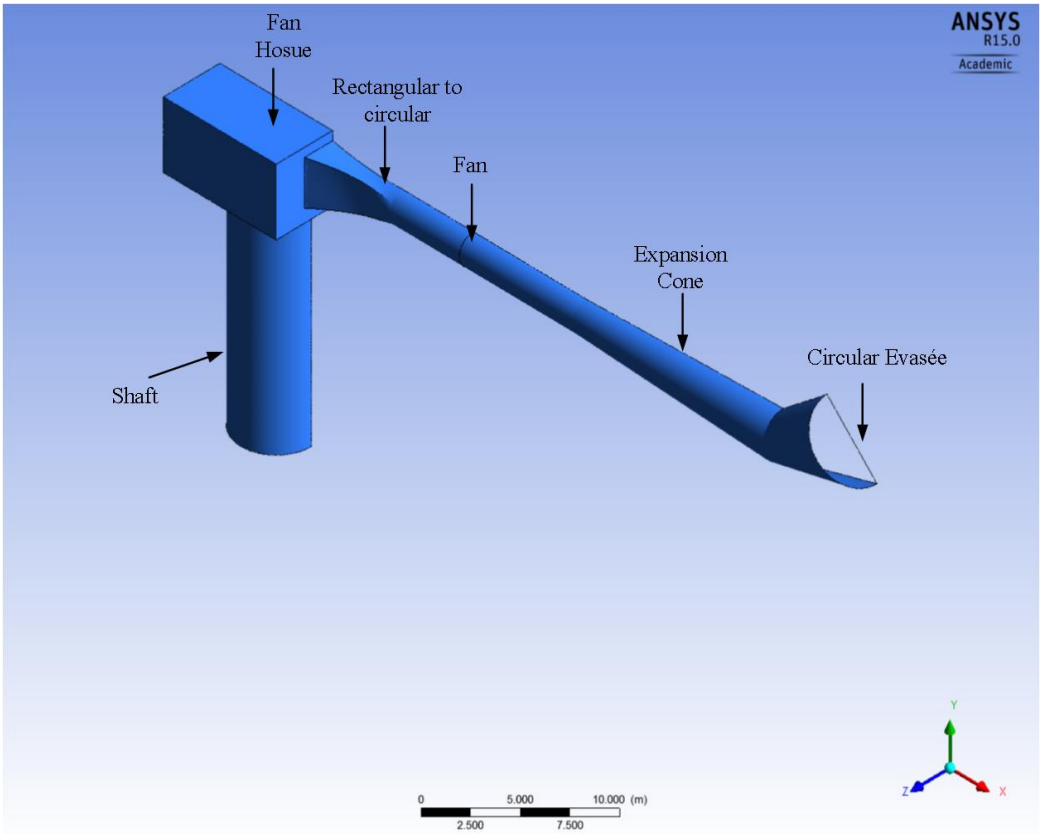

Figure 6.15 Geometry for the case 2

Table 6.7 Dimensions of various components

Components	Dimensions
Shaft	Diameter = 5m ,Length = 15 m
House	Length x Height x Width = 4 x 4 x 4 m^3
Fan	Diameter = 2 m
Expansion cone	Length = 14 m, inlet cone diameter = 2 m, and outlet cone diameter = 3 m
Evasée	Length = 8 m, diameter = 5 m Angle = 45 °

Same boundary conditions are used for the base case and case 1. The fan intake boundary condition was used to calculate the velocity for the given fan pressure for case 2, once the velocity is determined from the fan intake boundary conditions. A second simulation was performed for the case 2; velocity inlet boundary condition was used instead of the fan intake boundary condition.

6.3.2.1 Velocity Contours and Velocity Streamlines for Case 2

Figure 6.16 shows the velocity contours for this case. Figure 6.16 shows that the air recirculates near the outlet of the evasée. Furthermore, it shows most of the air volume in the evasée tends to exit from the center part of the outlet. The air flow near the upper and lower parts of the evasée is almost stagnant. The stagnation point means that the air at the upper and the lower sections of the evasée is spinning and recirculating. Figure 6.17, which depicts the velocity streamlines, highlights these flow patterns.

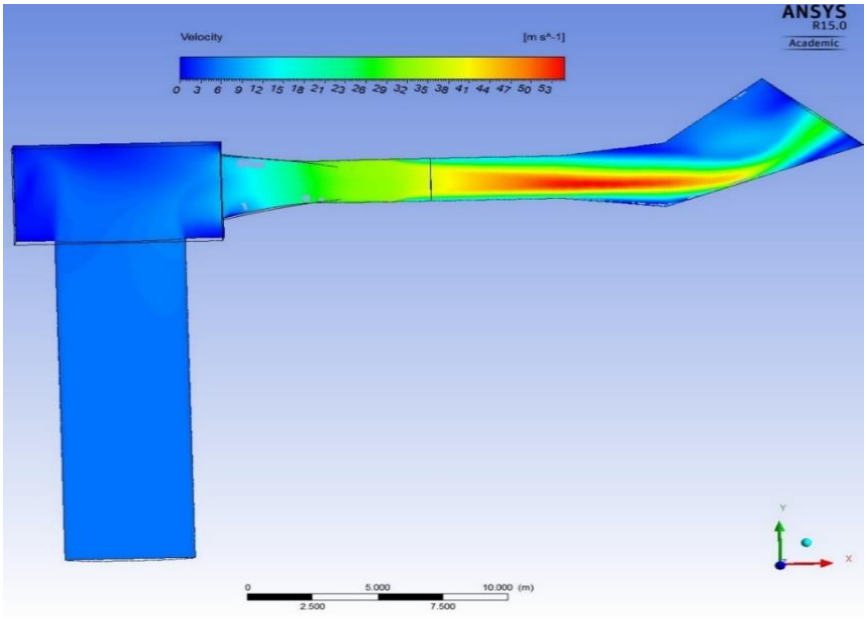

Figure 6.16 Velocity contours for the case 2

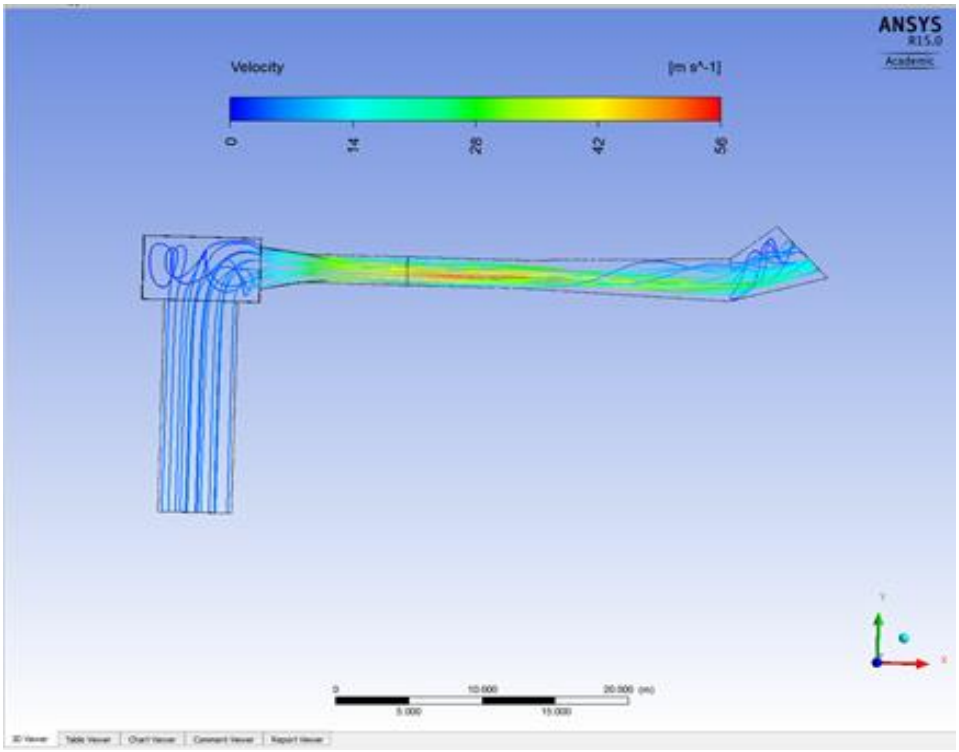

Figure 6.17 Velocity streamlines for the case 2

6.3.2.2 Pressure Profiles for Case 2

Figure 6.18 shows the pressure profiles for case 2. Based on these graphs it can be concluded that with an adequate evasée and ductwork design, the fan performance can be improved considerably. This is often translated by a reduction in shock losses and an increased flow capacity. In this case, such a change in evasée increased the fan capacity by 26 % (see subsection 6.3.4 for detail). However, it is difficult to accurately measure the increase in the fan capacity due to significant recirculation close to the evasée.

The 45 ° of the evasée also changes the flow direction, this change in the flow direction results in the pressure loss. From Figure 6.18 (pressure profiles for case 2), it can be concluded that most of the static pressure is recovered in the expansion cone.

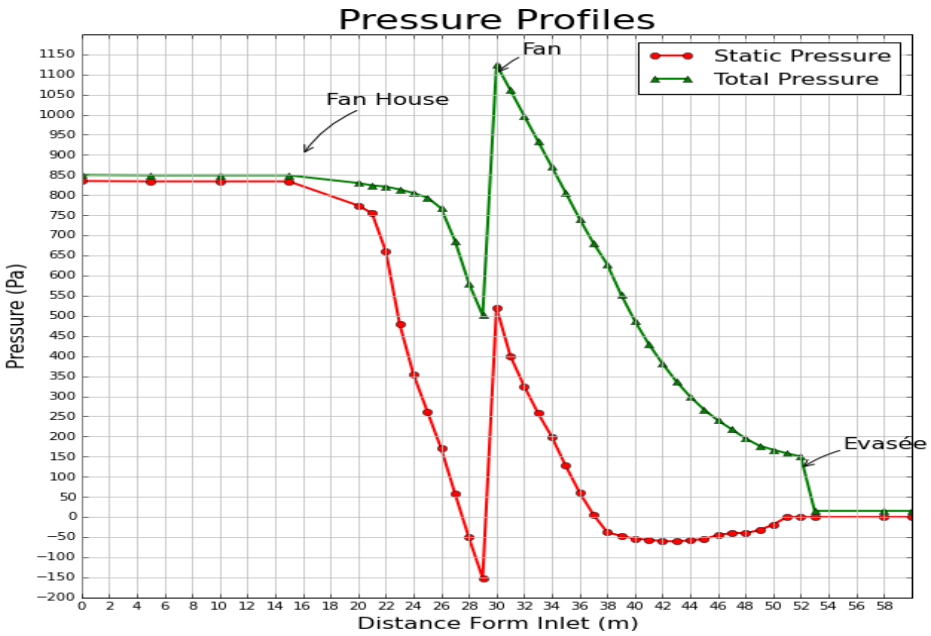

Figure 6.18 Pressure profiles for the case 2

6.3.2.3 Flowrate for Case 2

Based on the simulation results, the average inlet air velocity was estimated at 5 m/s and the average volume flowrate at 97 m^3/s. This means that the changes made to the geometry of the fan installation resulted in an increase in the flowrate of about 26 % when compared with the base case. Table 6.8 shows a summary of air velocities and flowrates at different sections of the model.

Table 6.8 Pressure and flow rate calculations for case 2

Distance from inlet (m)	**Static Pressure (Pa)**	**Total Pressure (Pa)**	**Velocity (m/s)**	**Area (m^2)**	**Air Quantity (m^3/s)**
0	835	850	5.00	20	97
5	834	849	5.00	20	97
10	834	849	5.00	20	97
15	834	849	5.00	20	98
20	774	830	9.56	12	114
25	354	794	26.80	3.152	84
30	520	1124	31.40	3.142	98
35	Turbulent	Turbulent	Turbulent	3.142	Turbulent
40	Turbulent	Turbulent	Turbulent	3.606	Turbulent
45	Turbulent	Turbulent	Turbulent	4.908	Turbulent
60	Turbulent	Turbulent	Turbulent	19.61	Turbulent

6.4 Conclusion

A set of CFD models has been developed to study the pressure losses at the fan house of an exhaust ventilation. A base case model was first formulated. The solution to the model showed that a significant portion of the fan pressure was lost at the fan evasée, mainly due to obstruction to the air path (shock losses). Then, the geometry model was modified and the effects of each change investigated through parametric studies. The results of these models were used to develop pressure profiles and to determine the effect of each change on fan performance.

The pressure profiles of the base case showed that more than 38 % of the fan pressure was lost at the fan house and in the vertical evasée (shock losses). To reduce these losses, two changes were made to the base model. For the first case, an expansion cone was inserted between the fan outlet and vertical evasée. For the second case, the rectangular evasée was replaced by a conical one and the sharp 90° elbow replaced by a 45° elbow.

The main purpose for conducting these studies was to evaluate alternatives to recover part of the pressure energy that was otherwise lost due to obstruction to the airflow at the fan discharge. For each case, pressure profiles were generated and the resulting graphs compared against those of the base case. Such a comparison showed that of the two parameters investigated, the installation of the conical evasée yielded lesser shock losses than inserting an expansion cone between the fan outlet and the rectangular evasée.

It is important that the length of conical evasée must be sufficient so that the air is fully developed at the conical evaseé. However, this result can still be improved by

combining these two parameters. From the pressure profiles of Figure 6.18, it can be concluded that a fan installation with proper ductwork and evasée designs (discussed in Chapter 2). This recommended design will reduce the formation of large eddies at the fan discharge, thus reducing the shock losses, and improving the overall fan efficiency.

CHAPTER 7

RECOMMENDATIONS AND CONCLUSION

This research work was conducted to identify methods for decreasing pressure losses associated with the installation of ventilation fans in underground mines. A review of the literature on fan installation for coal mines also reported a significant pressure loss as a result of improper installation design. This problem was also investigated by the ventilation research at the University of Utah, in ventilation surveys conducted at several U.S coal mines. In one of these mines, 49% of the fan pressure was lost on the surface, due to improper fan installation.

This study simulated two different fan installation systems using the ANSYS computational fluid dynamics software package. For case one, a blowing system was studied. For case two, an exhausting or suction system was simulated. To improve the design of the fan installation for both cases, the results of the simulations were studied and analyzed. In order to remove the source of the shock losses, the design of the fan installation was changed for each case. However, these improvements are based on certain limitations:

1. In fan installations, the fan pressure does not remain constant. It decreases with increased flow rate and vice versa. However, for this research, a fan with constant pressure was assumed.

2. In this study, an arbitrary fan pressure was specified in boundary conditions. The magnitude of the fan pressure depends on the mesh size. The only drawback of specifying an arbitrary fan pressure is that there will be a difference between the fan pressure obtained during the simulation and the fan pressure specified at the boundary conditions. This problem can be accounted by specifying fan details like a fan's characteristic curve, a fan motor's rpm, and the tangential velocity of air at the blade of the fan. These fan details can only be specified for an actual fan installation, and not for a schematic fan installation.

3. The k-ε turbulent model with enhanced wall treatment was used for all the parametric analysis. This wall treatment is applicable to any y-plus value; therefore, no calculations of y-plus values were performed in this study.

In spite of these limitations, the simulations showed the following design modifications that can be used to reduce pressure losses in ventilation fan installations: First, install an evasée with sufficient length to stabilize the air flow in the evasée. Second, avoid any abrupt changes in the flow direction between the fan and the ventilation drift and shaft. This can be done by installing carefully designed ductwork between the fan and the shaft. Following these guidelines requires the reconnaissance of the mine site and careful planning, to ensure that there is sufficient space for the fan installation.

In summary, this study is mainly concerned with identifying and diminishing the sources of shock losses. However, shock losses are not the only concern for mining engineers in the design of fan installations. These installations also generate high levels of noise. This noise pollution is accounted for in the location and design of ventilation fan

installations.

One reason for high noise levels in ventilation systems is the transformation of turbulence into unwanted acoustical energy. It is therefore recommended that the effect of the air velocity on the sound pressure level should be included in any future study.

REFERENCES

Conn, J.W., and Verakis, C. Harry., 1993, "System Design Analysis for Explosion Protection of Mine Fans," *Proceedings of the 6th US Mine Ventilation Symposium,* University of Utah, Salt Lake City, pp. 463-467.

Federal Register, 2014, Title 30 CFR Part 75 Mandatory Safety Standards – Underground Coal Mines. Subpart D – Ventilation, Code of Federal Regulations July 1 edition, http://www.msha.gov/30cfr/75.310.htm. August 2014.

Hartman, H.L., Mutmanshy, J.M., Ramani, R.V., and Wang, Y.J., 1997, *Mine Ventilation and Air Conditioning*, Third Edition, New York: John Wiley and Sons.

McPherson, M.J., 1993, *Subsurface Ventilation and Environmental Engineering*. London: Chapman and Hall.

Ray, Richard E., Jr. 1997, "Design Considerations for Main Exhaust Fan Systems at Underground Coal Mines," *Proceedings of the 6th International Mine Ventilation Congress,* Pittsburgh, PA. pp. 513-518.

TU, Jiyuan., YEOH, G.H., and LIU, C., 2008, *Computational Fluid Dynamics, A Practical Approach*, First Edition, Amsterdam: Butterworth- Heinemann.